Electronic Supplementary Information (ESI)

Structural Stability of BTTB based Metal-Organic Frameworks under Humid Conditions

Jagadeswara R. Karra[‡], *Himanshu Jasuja*[‡], *You-Gui Huang*[‡], *and Krista S. Walton**

School of Chemical and Biomolecular Engineering, Georgia Institute of Technology,

311 Ferst Dr. NW, Atlanta, GA 30332 USA

[‡]These authors contributed equally to this work.

*Corresponding author. E-mail: krista.walton@chbe.gatech.edu

Supplementary Index

A. Structure Description for CdBTTB (1), ZnBTTBBDC (2) MOFs.....S4
Table S1. Crystallographic data for compounds **1-2**.....S9
Table S2. Properties and thermal treatment conditions for Compounds **1-2**.....S10
Table S3. Selected Bond Lengths [Å] and Angles [°] for compound **1**.....S13
Table S4. Selected Bond Lengths [Å] and Angles [°] for compound **2**.....S14
Scheme S1. Coordination modes of BTTB ligand in compound **1**.....S10
Scheme S2. Coordination modes of BTTB and BDC ligands in compound **2**.....S11
Figure S1. Complicated network of compound **1**, herein described step by step.....S11
Figure S2. Self-penetrated network with carboxyl bridged {Cd_3} units in compound **1**…S12
Figure S3. Complicated network of compound **2**, herein described step by step S12
Figure S4. Coordination environments of Cd^{2+} ions in compound **1**.....S15
Figure S5. Coordination environments of Zn^{2+} ions in compound **2**.....S15
Figure S6. The structural fragment acting as 4-connected node in compound **2**.....S16
Figure S7. XRD patterns of compound **1**.....S16
Figure S8. XRD patterns of compound **2**.....S16
Figure S9. TGA traces of compound **1**.....S17
Figure S10. TGA traces of compound **2**.....S17
Figure S11. Nitrogen isotherm of activated **1** at 77 K.....S17
Figure S12. Nitrogen isotherm of activated **2** at 77 K.....S18
Figure S13. Photograph of single crystal of **1**.....S18
Figure S14. Photograph of single crystal of **2**.....S18
B. Structure Description for BTTB based Pillared MOFs (3, 4, 5, 6).....S19
Table S1. Crystallographic data for compounds **3-5**.....S26
Table S2. Properties and thermal treatment conditions for Compounds **3-5**.....S27
Table S3. Selected Bond Lengths [Å] and Angles [°] for compound **3**.....S30
Table S4. Selected Bond Lengths [Å] and Angles [°] for compound **4**.....S30
Table S5. Selected Bond Lengths [Å] and Angles [°] for compound **5**.....S31
Scheme S1. Cartoon representation of formation of pillared layer frameworks.....S27
Scheme S2. Organic ligands employed in this work.....S28
Figure S1. Structure of compound **4**, herein described step by step.....S28
Figure S2. Structure of compound **5**, herein described step by step.....S29
Figure S3. Simulated, as synthesized, chloroform exchange and activated XRD patterns of compound **4** and **6**.....S29
Figure S4. Coordination environment of Zn^{2+} ions in compound **4**.....S31
Figure S5. Coordination environment of Co^{2+} ions in compound **5**.....S32
Figure S6. Nitrogen isotherm of activated **3** at 77 K.....S32
Figure S7. Nitrogen isotherm of activated **4** at 77 K.....S33
Figure S8. Nitrogen isotherm of activated **5** at 77 K.....S33
Figure S9. Nitrogen isotherm of activated **6** at 77 K.....S33
Figure S10. As synthesized XRD patterns of compound **3** and **4**.....S34

Figure S11. Simulated, as synthesized, chloroform exchange and activated XRD patterns of compound **3**……S34
Figure S12. As synthesized XRD patterns of compound **5** and **6**……S34
Figure S13. Simulated, as synthesized, chloroform exchange and activated XRD patterns of compound **5**……S35
Figure S14. TGA traces of compound **3**……S35
Figure S15. TGA traces of compound **4**……S35
Figure S16. TGA traces of compound **5**……S36
Figure S17. TGA traces of compound **6**……S36
Figure S18. Photograph of single crystal of **3**……S36
Figure S19. Photograph of single crystal of **4**……S37
Figure S20. Photograph of single crystal of **5**……S37
Figure S21. Photograph of single crystal of **6**……S37
Figure S22. Repeatability of water adsorption isotherms of **4**……S38

A. Structure Description for CdBTTB, ZnBTTBBDC MOFs

Two porous metal-organic frameworks $\{[Cd_3(HBTTB)_2\cdot(H_2O)_2]\cdot(DEF)_4(H_2O)_6\}_n$ (**1**) and $\{[Zn_6(BTTB)_3(H_2BDC)(H_2O)_4]\cdot(DEF)\}_n$ **(2)** based on a long tetragonal bridging ligand 4,4',4",4"'-benzene-1,2,4,5-tetrayltetrabenzoic acid (H_4BTTB) have been synthesized under solvothermal conditions. Both compounds show self-penetration, compound **1** exhibits extraordinary assembly from a 3D PtS net to a 3D self-penetrating ***fla*** net, while compound **2** is a 3D framework composed of carboxyl connected interpenetrated PtS nets. Compound **1** and compound **2** have Brunauer-Emmett-Teller (BET) surface areas of 415m^2/g and 441 m^2/g, respectively.

Experimental Section

Materials and methods. All commercially available chemicals and solvents were of reagent grade and were used as received without further purification. Thermogravimetric analyses (TGA) were carried out in the temperature range of 25-700 ˚C on a NETSZCH TG/Mass spectrometry analyzer under helium with a heating rate of 5 ˚C/min. Powder X-ray diffraction patterns (PXRD) were recorded on a X'Pert X-ray PANalytical diffractometer with an X'accelerator module using Cu Kα (λ = 1.5418 Å) radiation at room temperature, with a step size of 0.02˚ in 2θ. Elemental analysis was performed by Desert Analytics, Arizona. CCDC 986372-986373 contain the supplementary crystallographic data for **1** and **2**.

Synthesis of MOFs:

$\{[Cd_3(HBTTB)_2\cdot(H_2O)_2]\cdot(DEF)_4(H_2O)_6\}_n$ (1) A mixture containing $Cd(NO_3)_2.4H_2O$ (61.6 mg, 0.2 mmol), H_4BTTB (55.8 mg, 0.1 mmol), PDC (2, 5-pyridine dicarboxylic acid , 16.7 mg, 0.1mmol), 2 mL DEF, 2 mL ethanol, 1 mL water, and 2 drops of 1N HCl was sealed in a 23 mL Teflon lined stainless steel container and heated at 100 ˚C for 4 days. After cooling to room temperature, colorless block shaped crystals of **1** were obtained (Figure S13). Subsequent synthesis without PDC produced the title compound, thus suggesting merely a spectator role for the PDC. Elemental analysis (%) Calcd: C 52.76 H 5.22 N 2.79 Found : C 52.2 H 5.13 N 2.61. Yield: 57 mg (42 % based on Cd).

$\{[Zn_6(BTTB)_3(H_2BDC)(H_2O)_4]\cdot(DEF)\}_n$ (2) A mixture containing $Zn(NO_3)_2.6H_2O$ (59.4 mg,

0.2 mmol), H_4BTTB (58.8 mg, 0.1 mmol), BDC (16.6 mg, 0.1 mmol), 2 mL DEF, 2 mL ethanol, 1 mL water , and 2 drops of 1N HCl was sealed in a 23 mL Teflon lined stainless steel container and heated at 100 ˚C for 4 days. After cooling to room temperature, colorless block shaped crystals of **2** were obtained (Figure S14). Elemental analysis (%) Calcd: C 57.6 H 4.6 N 2.06 Found : C 57.3 H 4.84 N 2.12. Yield: 35.7 mg (40% based on Zn).

X-ray crystallography. Single-crystal X-ray data of **1** and **2** were collected on a Bruker APEX II CCD sealed tube diffractometer by using Mo-*K*α and Cu-*K*α radiation respectively with a graphite monochromator. MOF crystals were mounted on nylon CryoLoops with Paratone-N. The structures were solved by direct methods and refined on F^2 by full-matrix least-squares using the using the SHELXTL-97 software suite. Anisotropic thermal parameters were refined for all non-hydrogen atoms; hydrogen atoms were refined isotropically as riding atoms. Some of the hydrogen atoms could not be resolved, and thus were not included in the analysis. For **CdBTTB**, we refined the structure by twin law, the absolute configuration of the crystal cannot be determined. For **ZnBTTBBDC**, the BDC ligand and terminal water molecules in the structure are in partial occupancy. To determine the occupancy, we refined them freely and found the occupancy for both is about 0.5, then refined the structure fixing their occupancy to be 0.5. Some restrains were made on BDC ligand. For both compounds, the routine SQUEEZE was used to remove the very diffuse electron density associated with the disordered solvent molecules in the pores. Pertinent crystallographic data and structure refinement parameters are summarized in Table S1.

Structural description

$\{[Cd_3(HBTTB)_2\cdot(H_2O)_2]\cdot(DEF)_4(H_2O)_6\}_n$ (1) Single–crystal X-ray diffraction reveals that compound **1** crystallizes in the chiral space group $P222_1$ and the asymmetric unit contains three Cd(II) ions, four half BTTB ligands, two coordinated H_2O molecules. All the Cd(II) ions are bonded by six oxygen atoms in a distorted octahedral geometry with Cd-O bond lengths in the range of 2.225-2.531 Å. Both Cd1 and Cd3 are coordinated by six oxygen atoms from four different BTTB ligands, while Cd2 is coordinated by six oxygen atoms with four from four different BTTB ligands and the other two from terminal H_2O molecules (Figure S4). In the structure of compound **1**, four crystallographically independent BTTB ligands exist, adopting

(κ^2)-(κ^2)-$(\kappa^1$-$\kappa^1)$-$(\kappa^1$-$\kappa^1)$-μ_6, $(\kappa^1$-$\kappa^1)$-$(\kappa^1$-$\kappa^1)$-$(\kappa^1$-$\kappa^1)$-$(\kappa^1$-$\kappa^1)$-μ_8, (κ^1)-(κ^1)-(κ^2)-(κ^2)-μ_4, (κ^2)-(κ^2)-(κ^2)-(κ^2)-μ_4, coordination mode, respectively (Scheme S1).

The network of compound **1** is very complicated, herein we described it step by step. Cd1 and Cd2 centers are bridged by carboxyl groups from $BTTB_A$ and $BTTB_C$ to form dinuclear units which are further connected by spacers of $BTTB_A$ and $BTTB_C$ to give rise to a 3D framework with very big channels (Figure S1a). By treating both $\{Cd_2\}$ unit and BTTB ligand as 4-connected nodes, the 3D framework can be simplified as a PtS net (Figure S1b). On the other hand, Cd3 centers are connected by $BTTB_B$ and $BTTB_D$ to give rise to a similar framework (Figure S1c) which also can be simplified as a PtS net (Figure S1d). Above two independent frameworks connect to each other by Cd2-O13 bonds forming a self-penetrated network with carboxyl bridged $\{Cd_3\}$ units (Figure S2). In the view of topology, by treating $\{Cd_3\}$ unit and BTTB ligand as nodes, the whole framework can be viewed as a (4-8)-connected ***fla*** net (Figure S2c). As a result of self-penetration, the big channels in a single PtS net are partially blocked, producing channels interconnected in three-dimensions with pore sizes of 5.413 Å along [1 0 0] direction, 5.413 Å along [0 1 0] direction and 7.773 Å along [0 0 1] direction (taking into account the van der Waals radii of atoms), which are available for guest accommodation and exchange. As estimated by PLATON[1], the void volume in compound **1** is 52% of unit cell volume. The channels are occupied by H_2O, DEF and ethanol molecules. Water molecules interact weakly with the central Cd(II) ion, and removal of water molecules generates exposed cadmium sites inside the pores, which can act as interaction sites between the host and guest molecules.

$\{[Zn_6(BTTB)_3(H_2BDC)(H_2O)_4]\cdot(DEF)\}_n$ (2) Compound **2** crystallizes in the space group *P*-1, but is a 3D framework composed of carboxyl connected interpenetrated PtS nets. The asymmetric unit contains six crystallographically independent Zn(II) ions in the form of three $\{Zn_2\}$ dinuclear units, three BTTB ligands and one BDC ligand. The coordination modes of Zn(II) ions show diversity. Zn1, Zn3and Zn6 are coordinated by four oxygen atoms in a tetrahedral geometry, while Zn2, Zn4and Zn5 are in a distorted octahedral geometry bonded by six oxygen atoms (Figure S5). The bond lengths of Zn-O range from 1.901 Å to 2.400 Å. Three crystallographically independent BTTB ligand, $BTTB_A$, $BTTB_B$, $BTTB_C$ adopts $(\kappa^1$-$\kappa^1)$-(κ^1)-$(\kappa^1$-$\kappa^1)$-(κ^1)-μ_6, (κ^2)-$(\kappa^1$-$\kappa^1)$-(κ^2)-$(\kappa^2$-$\kappa^1)$-μ_6, $(\kappa^1$-$\kappa^1)$-$(\kappa^1$-$\kappa^1)$-(κ^2)-$(\kappa^1$-$\kappa^1)$-μ_7 coordination mode, respectively (Scheme S2).

Each BTTB ligand binding to four {Zn_2} dinuclear units and each {Zn_2} dinuclear unit connecting to four BTTB ligands, gives rise to a 3D framework with huge channels along [0 1 0] direction (Figure S3a). In the framework, two {Zn_2} dinuclear units formed by Zn5 and Zn6 atoms are connected together by two $BTTB_A$ ligands to form a structural fragment (Figure S6). In the view of topology, above structural fragment, the other two {Zn_2} dinuclear units and $BTTB_B$, $BTTB_C$ can be treated as 4-connected nodes, thus the 3D framework can be simplified as a PtS net (Figure S3b). Two independent PtS nets interpenetrate resulted in the huge channels along [0 1 0] direction partially blocked (Figure S3d). Finally, the BDC ligands connect the interpenetrated nets together with one of the carboxyl groups in a μ_2-η^1:η^1 mode to form a single framework with self-penetration (Figure S3c). Calculation with PLATON[1] shows that the effective volume for the inclusion is 44% of the crystal volume in compound **2**. The channel sizes are 4.243 Å along [0 0 1] direction and 6.507 Å along [0 1 0] direction and are filled with guest solvent molecules.

Surface area, bulk phase purity and thermal properties

After synthesis, compounds **1** and **2** were solvent exchanged with chloroform, dichloromethane, or methanol, and activated at 150 ˚C overnight under vacuum. However, solvent exchange always gave poor surface areas. The activation temperatures of compound **1** and compound **2** were varied from 100 to 350 ˚C in increments of 50 ˚C, and their activation times were varied from an hour to overnight under vacuum. BET surface areas were measured after each activation process. For compound **1**, the largest surface area was obtained when the sample was activated under vacuum at 300 ˚C for an hour. In case of compound **2**, the largest surface area was obtained when the sample was activated under vacuum at 250 ˚C for an hour.

Table S2 shows the summary of activation procedure for both MOFs along with their accessible surface areas calculated from the crystal structure.[2] The obtained BET surface areas for both compounds **1** and **2** are much smaller than those calculated geometrically from the perfect crystal structure with nitrogen molecule as a probe.[2] As activation for these samples was done near their decomposition temperatures for a short period of time, it is quite possible that some of the pores have collapsed, or there may be defects or trapped residual solvent molecules present in the samples. Note that TGA measurements (Figure S9-S10) alone cannot be used to determine the stability of an open structure since it may collapse without a notable change in weight.

The N_2 adsorption/desorption isotherms measured at 77 K for both compounds **1** and **2** (Figure S11-S12) reveal typical Type-I behavior, as expected for microporous materials. Fitting the Brunauer-Emmett-Teller (BET) equation to their respective N_2 adsorption isotherms within the range $0.007<P/P_0<0.03$ gives an estimated surface area of 415 m^2/g for compound **1** and 441 m^2/g for compound **2**. The Dubinin-Astakhov (DA) equation gives an estimated pore volume of 0.19 cm^3/g for compound **1** and 0.21 cm^3/g for compound **2**. Both compounds are stable in air and insoluble in water and most of the common organic solvents such as chloroform, methanol, acetone, toluene, and dimethyl formamide.

In order to confirm the phase purity of the bulk materials **1** and **2**, PXRD experiments (Figure S7-S8) were carried out. All major peaks of as-synthesized powder X-ray patterns (PXRDs) agree reasonably well with that of simulated PXRD patterns. There are some missing or extra minor peaks that could be attributed to the impurities present in these samples.

In all the activated samples, there was a loss of transparency and single crystallinity. Some peaks were lost after activation, with the major framework structure maintained. This suggests that some of the pores have partially collapsed in these MOFs, which could be the reason for their lower surface areas. Upon resolvation in DEF and water, the PXRD pattern of compound **2** was regenerated. For compound **1**, the structure did not change upon resolvation and was the same as its activated sample.

Compound **1** displays a thermal stability of ~ 350 ˚C. A steady weight loss of ~ 18%, corresponding to removal of coordinated water molecules and uncoordinated solvent molecules is seen between room temperature and 300 ˚C, and a rapid weight loss beyond 400 ˚C suggests the framework breaks down due to the decomposition of BTTB ligand. Removal of guest molecules from compound **1** was done at 300 ˚C for 1 hr, and this was confirmed from the thermogravimetric data and PXRD data of activated sample of compound **1**. Compound **2** undergoes a steady weight loss of ~ 10 %, from 100 to 300 ˚C and then reaches a small plateau region, and beyond 350 ˚C, a rapid weight loss occurs. The weight loss of ~ 10 % corresponds to removal of coordinated and uncoordinated solvent molecules. Removal of guest molecules from Compound **2** was done at 250 ˚C for 1 hr and this was confirmed from the thermogravimetric data and PXRD data of activated sample of Compound **2**.

REFERENCES

(1) Spek, A.L. **2005**, PLATON, A Multipurpose Crystallographic Tool, Utrecht University, Utrecht, The Netherlands.

(2) Duren, T.; Millange, F.; Frey, G.; Walton, K. S.; Snurr, R. Q. *J. Phys. Chem. C* **2007**, 111, 15350.

Table S1. Crystallographic data for compounds **1-2**

Compound	**1**	**2**
Formula	$C_{68}H_{40}Cd_3O_{18}$	$C_{106}H_{60}O_{28}Zn_6$
*F*w	1481.17	2173.73
Crystal size(mm)	0.10 × 0.10 × 0.07	0.12 × 0.12 × 0.06
Space group	*P2221*	*P-1*
a(Å)	28.677(2)	15.8225(5)
b(Å)	15.8555(11)	16.8196(5)
c(Å)	21.4018(15)	28.4760(11)
$\alpha(^o)$	90	96.700(2)
$\beta(^o)$	90	100.221(3)
$\gamma(^o)$	90	109.597(2)
$V(Å^3)$	9731.1(12)	6898.0(4)
Z	4	2
$\lambda(K\alpha)$(Å)	0.71703	1.54178
$D_c(g/cm^3)$	1.009	1.045
$\mu(mm^{-1})$	0.696	1.618
T(K)	296(2)	173(2)
Total reflections	208073	61381
Unique data collected	18334	20992
Observed reflections	15215	13636
*R*int	0.0788	0.0435
Parameters	802	1333
R_1, *w*R(I > 2σ(I))[a]	0.0428, 0.1228	0.1009 , 0.3001
R_1, *w*R(all data)[b]	0.0524, 0.1265	0.1205 , 0.3230
$w=1/[\sigma^2(F_0^2)+(aP)^2+Bp]$	a= 0.0974, b= 0.0000	a= 0.2000, b= 0.0000
Goodness-of-fit-on F^2	0.92	1.198
$\Delta\rho_{min}$ and $\Delta\rho_{max}$(e $Å^{-3}$)	-1.700, 3.822	-0.927 , 1.284

[a] $R = \sum||F_0|-|F_c||/\sum|F_0|$

[b] $wR = |\sum w(F_0-F_c)^2/\sum w(F_0^2)^2|^{1/2}$

Table S2. Properties and thermal treatment conditions for Compounds **1-2**

MOF	Pore size (Å)	Pore volume (cm^3/g)	BET surface area (m^2/g)	Activation process (under vacuum)	Thermal stability	Features	Calculated Accessible Surface Area (m^2/g)
1	5.413	0.19	415	300 ˚ C (1h)	350 ˚C	3-D pore system, open Cd sites	2180
2	4.243	0.209	441	250 ˚ C (1h)	350 ˚C	2-D pore system, open Zn sites	1114

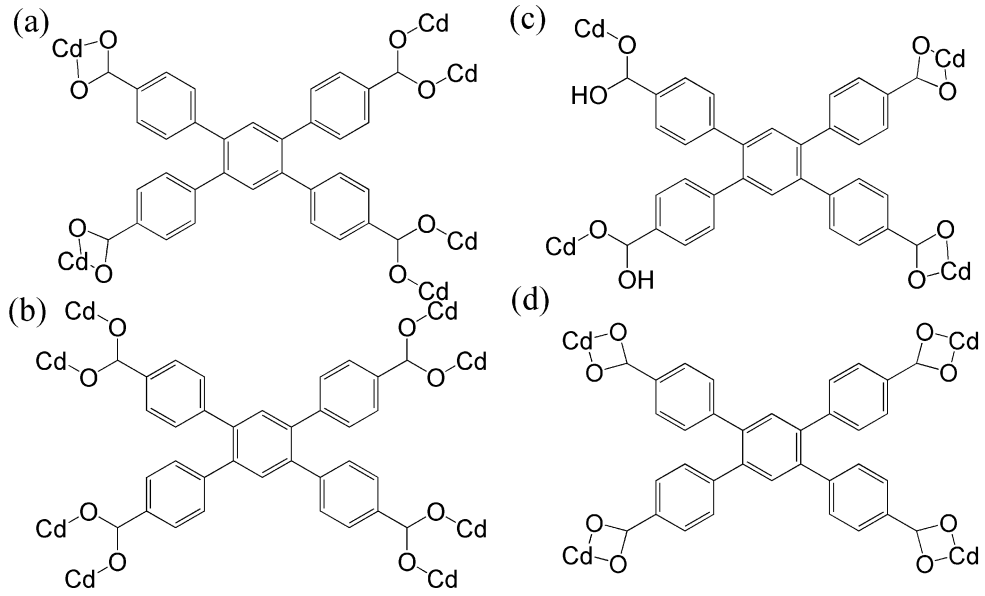

Scheme S1. Coordination modes of BTTB ligand in compound **1**.

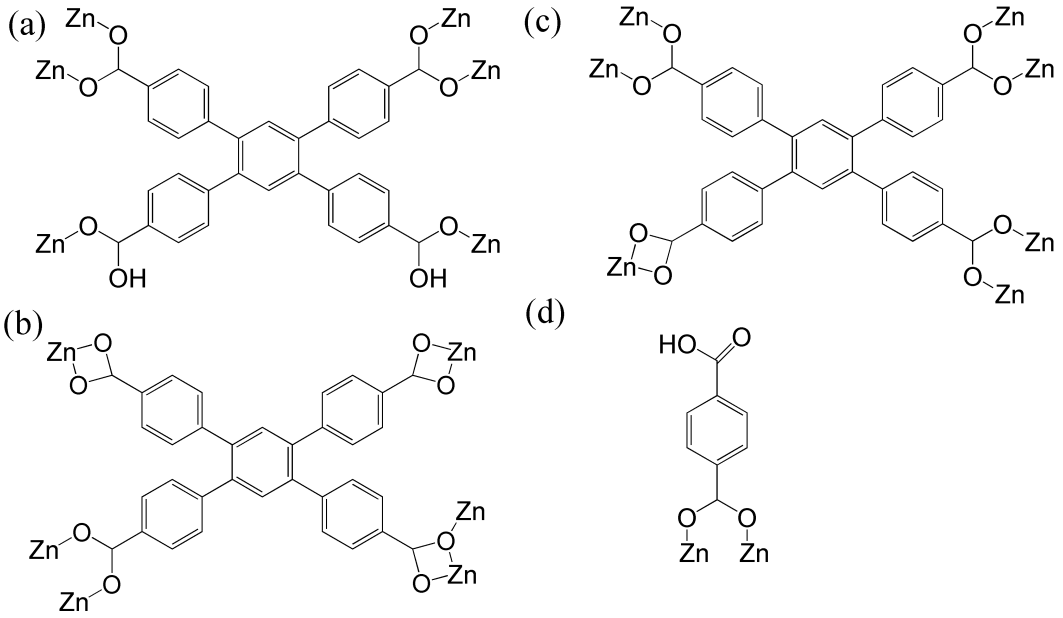

Scheme S2. Coordination modes of BTTB and BDC ligands in compound **2**.

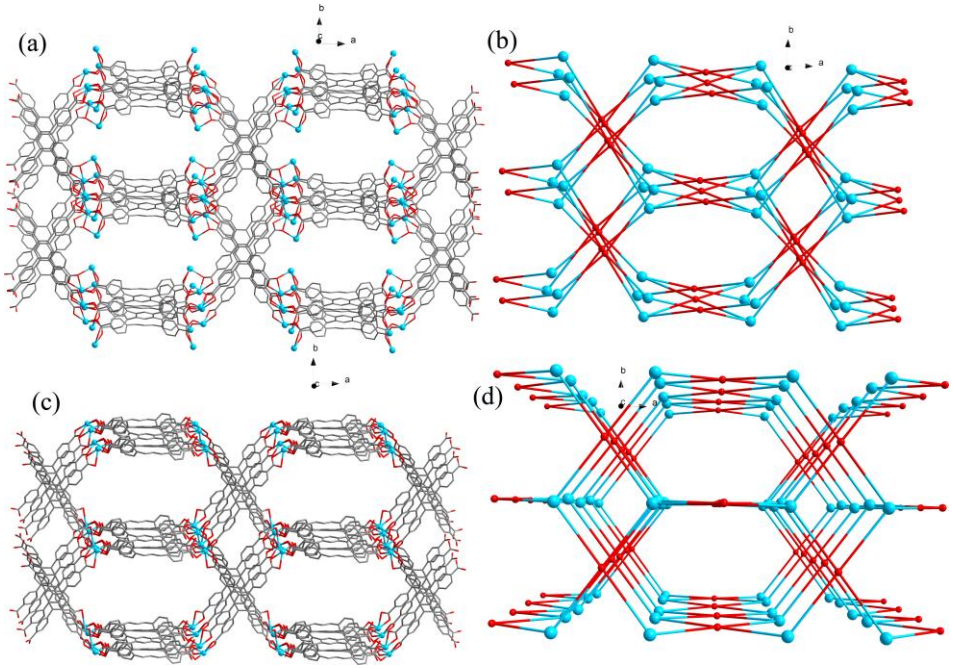

Figure S1. (a) The 3D framework with very big channels constructed by $BTTB_A$ and $BTTB_C$ bridged $\{Cd_2\}$ dinuclears in compound **1**. (b) Topological view of the framework constructed by $BTTB_A$ and $BTTB_C$ bridged $\{Cd_2\}$ dinuclears with PtS net. (c) The 3D framework constructed by $BTTB_B$ and $BTTB_D$ bridged {Cd} ions in compound **1**. (d) Topological view of the framework constructed by $BTTB_B$ and $BTTB_D$ bridged {Cd} ions.

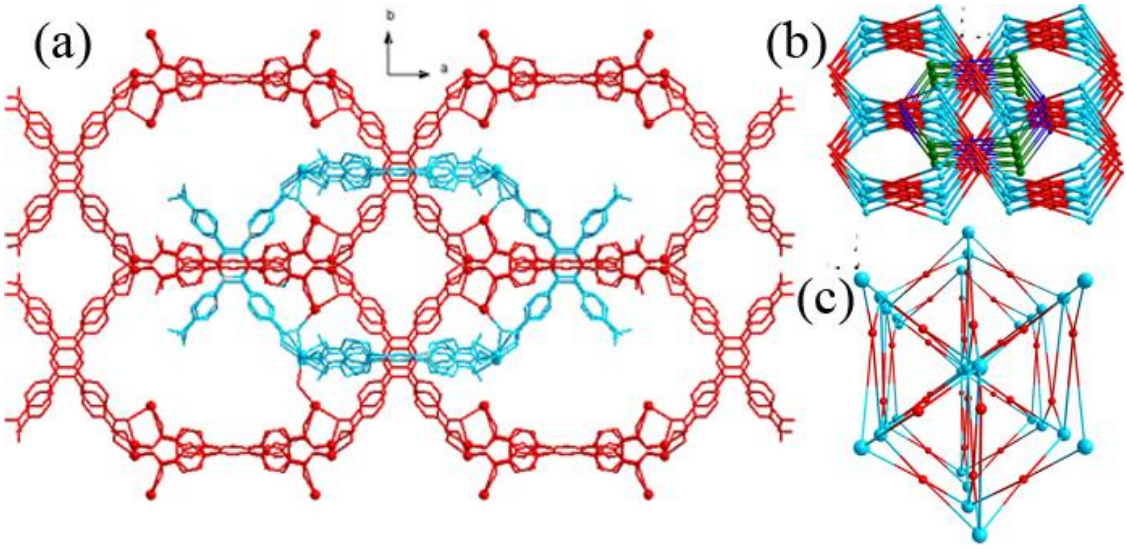

Figure S2. (a) The self-penetrated framework of Compound **1**. (b) Topological view of the penetration of two independent PtS nets in compound **1**. (c) The ***fla*** net of compound **1**.

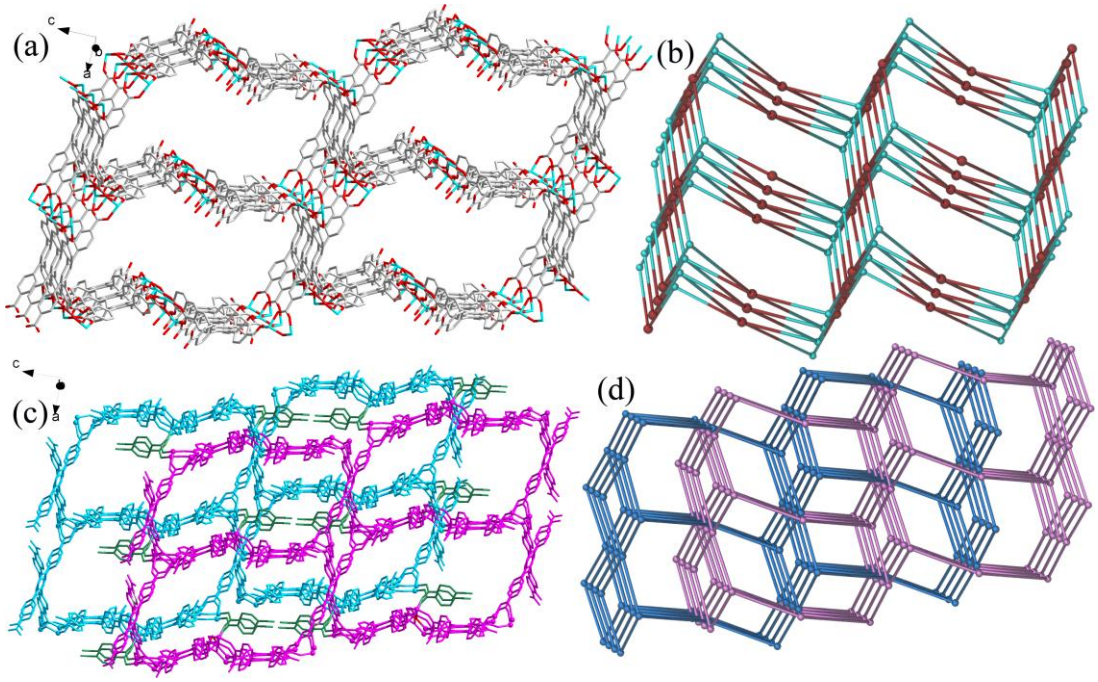

Figure S3. (a) A single 3D framework with big channels along *b* axis in compound **2**. (b) Topological view of the single framework with PtS net. (c) The BDC bridged two interpenetrated frameworks of compound **2**. (d) Topological view of the interpenetrated nets in compound **2**.

***Table S3*. Selected bond lengths [Å] and angles [°]for 1.**

Compound **1** (bond)			
Cd1—O11^{i}	2.212 (2)	Cd2—O12^{i}	2.329 (2)
Cd1—O9	2.235 (2)	Cd2—O13	2.327 (2)
Cd1—O1	2.257 (2)	Cd3—O5	2.225 (2)
Cd1—O3^{ii}	2.306 (2)	Cd3—O14	2.300 (2)
Cd1—O4^{ii}	2.403 (2)	Cd3—O7^{iii}	2.314 (2)
Cd1—O2	2.531 (2)	Cd3—O16^{iv}	2.333 (3)
Cd2—O17	2.235 (2)	Cd3—O15^{iv}	2.451 (3)
Cd2—O10	2.236 (2)	Cd3—O8^{iii}	2.484 (2)
Cd2—O18	2.258 (3)		
(angle)			
O11^{i}—Cd1—O9	90.30 (9)	O10—Cd2—O13	108.65 (8)
O11^{i}—Cd1—O1	112.15 (9)	O18—Cd2—O13	81.18 (10)
O9—Cd1—O1	100.17 (10)	O12^{i}—Cd2—O13	104.63 (8)
O11^{i}—Cd1—O3^{ii}	88.80 (8)	O17—Cd2—O1	89.97 (8)
O9—Cd1—O3^{ii}	111.43 (9)	O10—Cd2—O1	84.26 (8)
O1—Cd1—O3^{ii}	142.05 (8)	O18—Cd2—O1	84.54 (10)
O11^{i}—Cd1—O4^{ii}	143.54 (8)	O12^{i}—Cd2—O1	91.98 (8)
O9—Cd1—O4^{ii}	94.65 (9)	O13—Cd2—O1	160.06 (7)
O1—Cd1—O4^{ii}	102.48 (8)	O5—Cd3—O14	127.20 (8)
O3^{ii}—Cd1—O4^{ii}	55.83 (8)	O5—Cd3—O7^{iii}	94.55 (9)
O11^{i}—Cd1—O2	107.98 (9)	O14—Cd3—O7^{iii}	94.59 (9)
O9—Cd1—O2	152.71 (9)	O5—Cd3—O16^{iv}	140.83 (10)
O1—Cd1—O2	54.58 (8)	O14—Cd3—O16^{iv}	85.00 (9)
O3^{ii}—Cd1—O2	89.59 (8)	O7^{iii}—Cd3—O16^{iv}	105.46 (10)
O4^{ii}—Cd1—O2	82.69 (9)	O5—Cd3—O15^{iv}	104.28 (9)
O17—Cd2—O10	166.62 (9)	O14—Cd3—O15^{iv}	81.09 (10)
O17—Cd2—O18	104.69 (11)	O7^{iii}—Cd3—O15^{iv}	159.23 (10)
O10—Cd2—O18	86.81 (10)	O16^{iv}—Cd3—O15^{iv}	54.08 (11)
O17—Cd2—O12^{i}	86.32 (9)	O5—Cd3—O8^{iii}	79.20 (9)
O10—Cd2—O12^{i}	81.84 (9)	O14—Cd3—O8^{iii}	143.17 (10)
O18—Cd2—O12^{i}	168.41 (10)	O7^{iii}—Cd3—O8^{iii}	54.13 (9)
O17—Cd2—O13	80.33 (8)	O16^{iv}—Cd3—O8^{iii}	85.73 (9)

Symmetry codes: (i) 2-x, y, 3/2-z; (ii) x, -1+y, z; (iii) 1-x, y, 3/2-z; (iv) x, 1+y, z.

***Table S4*. Selected bond lengths [Å] and angles [°]for 2.**

Compound **2** (bond)			
Zn1—O2	1.901 (6)	Zn4—O11	1.991 (8)
Zn1—O16^{i}	1.949 (6)	Zn4—O21^{ii}	2.015 (6)
Zn1—O10	1.959 (6)	Zn4—O14^{i}	2.036 (11)
Zn1—O25	1.943 (6)	Zn4—O31	2.147 (7)
Zn2—O1	1.950 (5)	Zn4—O13^{i}	2.400 (10)
Zn2—O9	1.986 (8)	Zn5—O23	1.980 (8)
Zn2—O15^{i}	1.969 (5)	Zn5—O26^{iii}	2.019 (8)
Zn2—O3^{ii}	2.123 (8)	Zn5—O7^{iv}	2.040 (7)
Zn2—O4^{ii}	2.198 (8)	Zn5—O5^{v}	2.132 (10)
Zn2—O29	2.320 (7)	Zn5—O6^{v}	2.294 (13)
Zn3—O17	1.901 (6)	Zn5—O8^{iv}	2.377 (12)
Zn3—O13^{i}	1.917 (10)	Zn6—O32	1.931 (8)
Zn3—O22^{ii}	1.936 (5)	Zn6—O24	1.923 (6)
Zn3—O12	1.945 (6)	Zn6—O19^{vi}	1.960 (8)
Zn4—O30	1.958 (7)	Zn6—O8^{iv}	1.974 (11)
(angle)			
O2—Zn1—O16^{i}	109.1 (3)	O21^{ii}—Zn4—O14^{i}	98.1 (4)
O2—Zn1—O10	115.0 (3)	O30—Zn4—O31	85.3 (3)
O16^{i}—Zn1—O10	117.0 (3)	O11—Zn4—O31	82.6 (3)
O2—Zn1—O25	107.7 (3)	O21^{ii}—Zn4—O31	177.5 (3)
O16^{i}—Zn1—O25	94.6 (3)	O14^{i}—Zn4—O31	84.4 (3)
O10—Zn1—O25	111.4 (4)	O30—Zn4—O13^{i}	165.3 (3)
O1—Zn2—O9	111.2 (3)	O11—Zn4—O13^{i}	84.8 (3)
O1—Zn2—O15^{i}	110.9 (3)	O21^{ii}—Zn4—O13^{i}	94.2 (3)
O9—Zn2—O15^{i}	94.4 (3)	O14^{i}—Zn4—O13^{i}	59.7 (4)
O1—Zn2—O3^{ii}	140.2 (3)	O31—Zn4—O13^{i}	87.3 (3)
O9—Zn2—O3^{ii}	94.1 (3)	O23—Zn5—O26^{iii}	95.5 (4)
O15^{i}—Zn2—O3^{ii}	96.7 (3)	O23—Zn5—O7^{iv}	146.9 (4)
O1—Zn2—O4^{ii}	90.9 (3)	O26^{iii}—Zn5—O7^{iv}	88.6 (3)
O9—Zn2—O4^{ii}	88.1 (4)	O23—Zn5—O5^{v}	92.6 (4)
O15^{i}—Zn2—O4^{ii}	155.3 (3)	O26^{iii}—Zn5—O5^{v}	159.0 (5)
O3^{ii}—Zn2—O4^{ii}	58.5 (3)	O7^{iv}—Zn5—O5^{v}	95.2 (3)
O1—Zn2—O29	77.9 (3)	O23—Zn5—O6^{v}	101.8 (3)
O9—Zn2—O29	170.0 (3)	O26^{iii}—Zn5—O6^{v}	97.7 (4)
O15^{i}—Zn2—O29	85.9 (3)	O7^{iv}—Zn5—O6^{v}	110.2 (4)
O3^{ii}—Zn2—O29	75.9 (3)	O5^{v}—Zn5—O6^{v}	61.6 (4)
O4^{ii}—Zn2—O29	87.5 (3)	O23—Zn5—O8^{iv}	90.1 (3)
O17—Zn3—O13^{i}	107.5 (4)	O26^{iii}—Zn5—O8^{iv}	98.3 (4)
O17—Zn3—O22^{ii}	120.2 (3)	O7^{iv}—Zn5—O8^{iv}	56.9 (3)
O13^{i}—Zn3—O22^{ii}	120.8 (3)	O5^{v}—Zn5—O8^{iv}	101.1 (4)
O17—Zn3—O12	104.9 (3)	O6^{v}—Zn5—O8^{iv}	159.0 (4)

O13^{i}—Zn3—O12	90.0 (4)	O32—Zn6—O24	104.9 (4)
O22^{ii}—Zn3—O12	108.0 (2)	O32—Zn6—O19^{vi}	110.5 (4)
O30—Zn4—O11	106.8 (3)	O24—Zn6—O19^{vi}	118.6 (4)
O30—Zn4—O21^{ii}	93.6 (3)	O32—Zn6—O8^{iv}	97.6 (4)
O11—Zn4—O21^{ii}	95.5 (3)	O24—Zn6—O8^{iv}	112.0 (4)
O30—Zn4—O14^{i}	106.8 (4)	O19^{vi}—Zn6—O8^{iv}	110.9 (6)
O11—Zn4—O14^{i}	142.7 (4)		

Symmetry codes: (i) 1+x, y, z; (ii) x, 1+y, z; (iii) 2-x, -y, 1-z; (iv) 1+x, y, 1+z; (v) 1+x, 1+y, 1+z; (vi) x, -1+y, z.

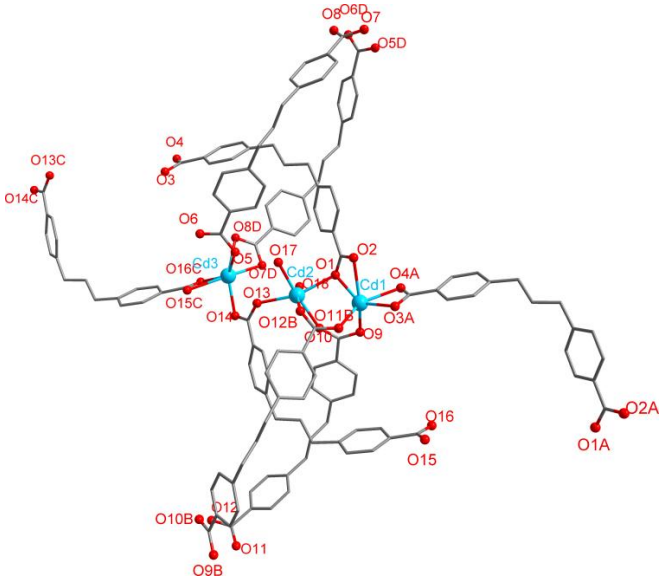

Figure S4. Coordination environments of Cd^{2+} ions in compound **1**. Symmetry codes: (A) x, y-1, z; (B) 2-x, y, 3/2-z; (C) x, 1+y, z; (D) 1-x, y, 3/2-z.

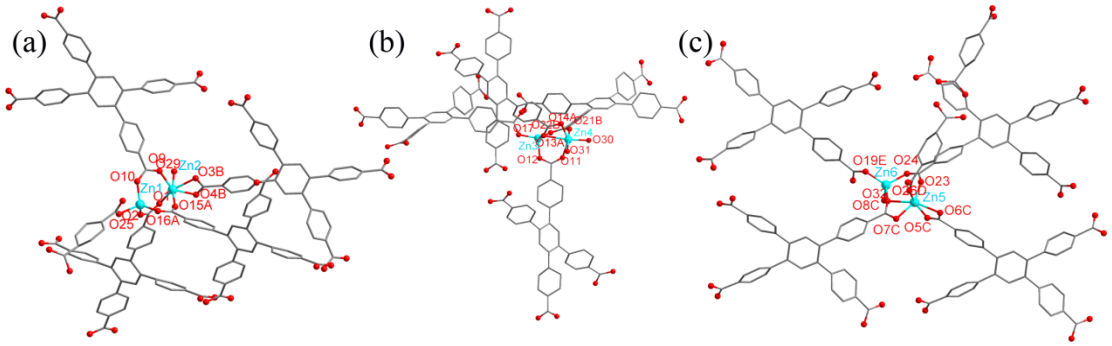

Figure S5. Coordination environments of Zn^{2+} ions in compound **2**. Symmetry codes: (A) 1+x, y, z; (B) x, 1+y, z; (C)1+x, y, 1+z; (D) 2-x, -y, 1+z; (E) x, y-1, z.

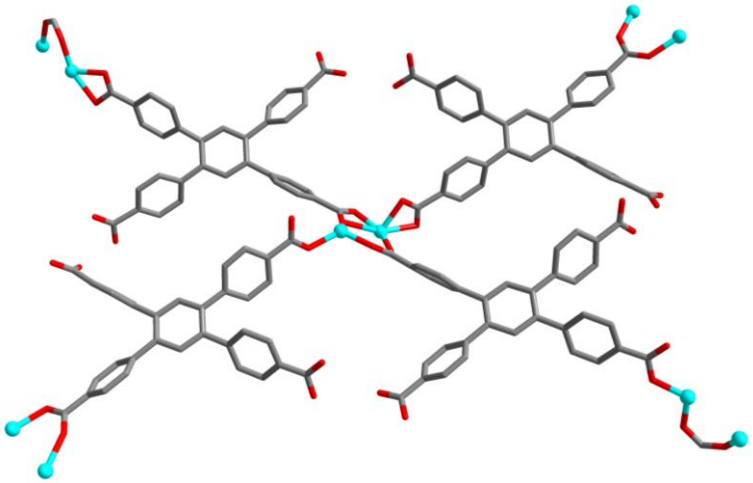

Figure S6. The structural fragment formed by $BTTB_A$ and $BTTB_C$ ligands linked $\{Zn_2\}$ dinuclear of Zn5 and Zn6 acting as a 4-connected node.

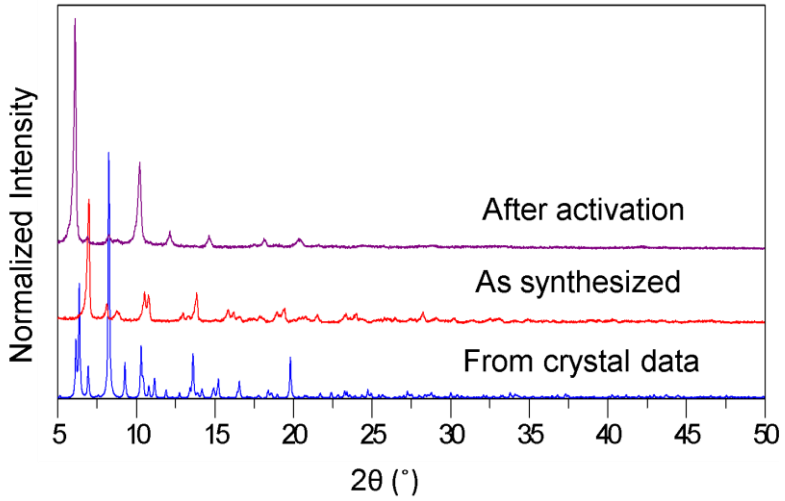

Figure S7. Simulated, as synthesized, and activated powder X-ray diffraction patterns of **1**

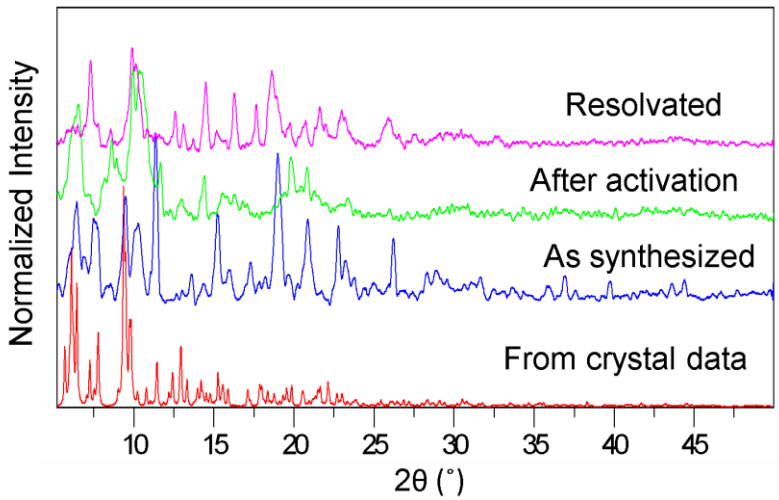

Figure S8. Simulated, as synthesized, activated, and resolvated powder X-ray diffraction patterns of **2**.

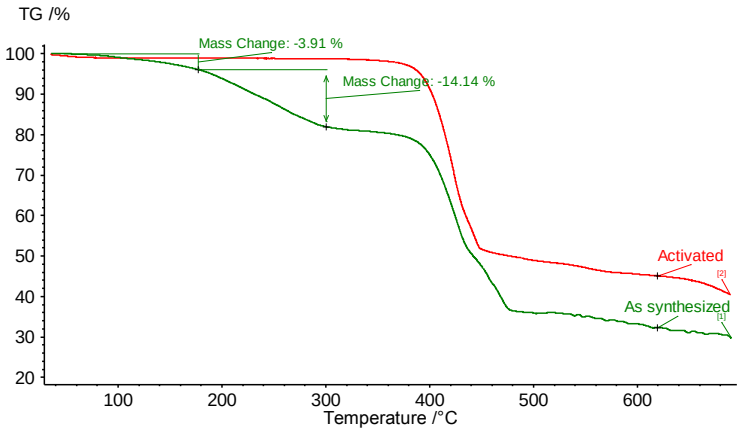

Figure S9. TGA trace of **1**.

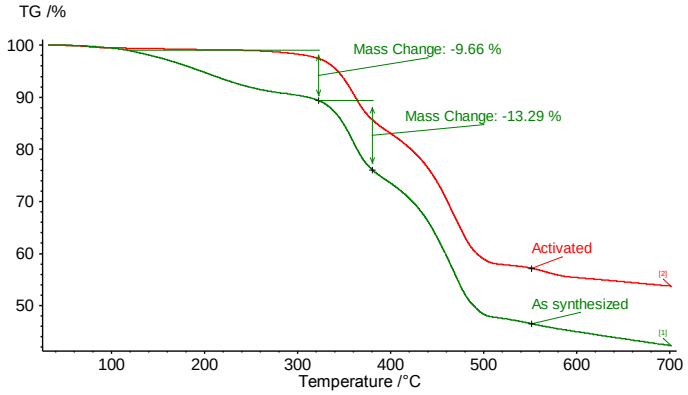

Figure S10. TGA trace of **2**.

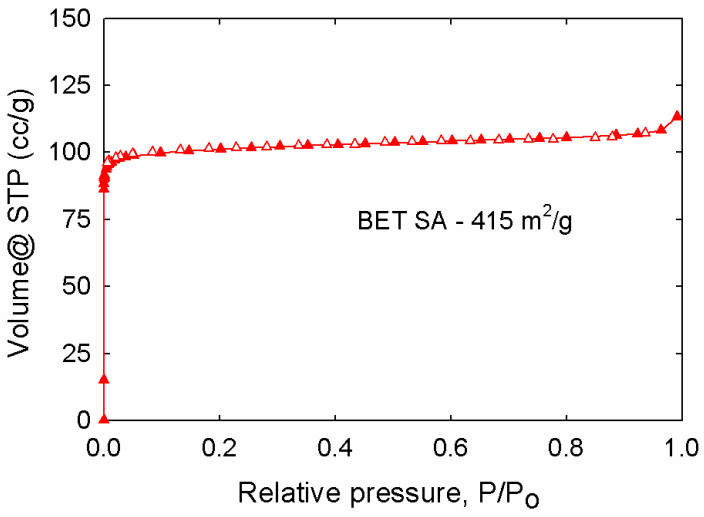

Figure S11. Nitrogen isotherm of activated **1** at 77 K (closed symbols – adsorption, open symbols – desorption).

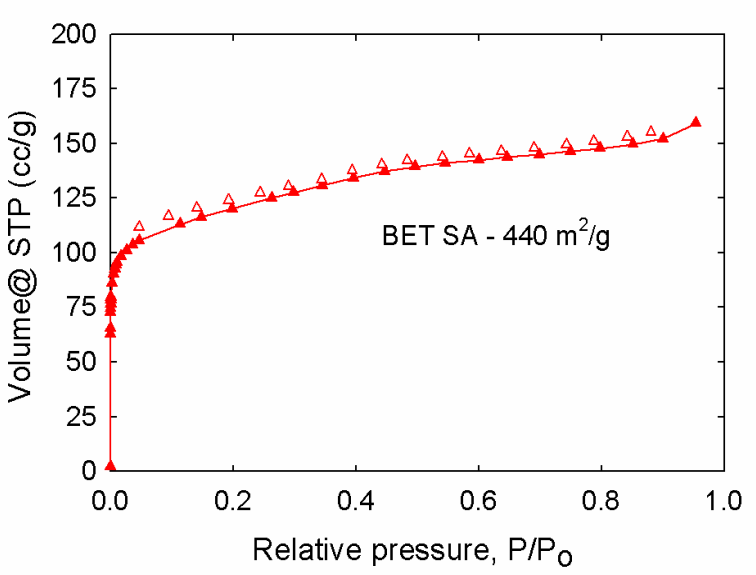

Figure S12. Nitrogen isotherm of activated **2** at 77 K (closed symbols – adsorption, open symbols – desorption).

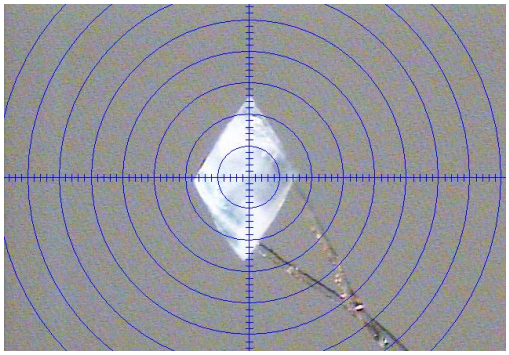

Figure S13. Photograph of single crystal of **1** (size (mm) – 0.1 x 0.1 x 0.07).

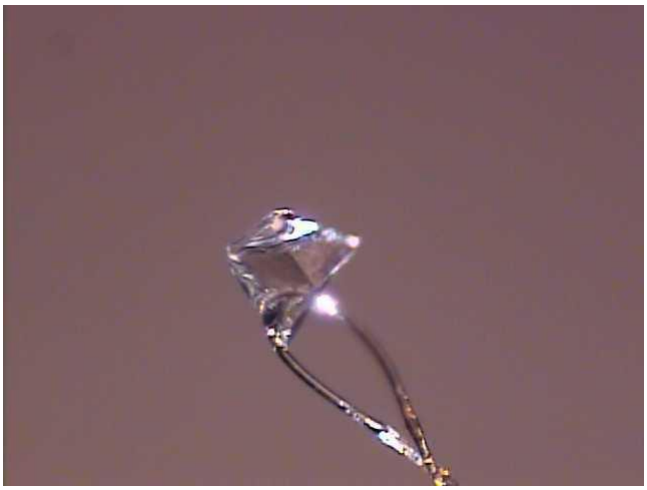

Figure S14. Photograph of single crystal of **2** (size (mm) – 0.12 x 0.12 x 0.06).

B. Structure Description for BTTB based Pillared MOFs

A series of isostructural porous metal-organic frameworks (MOFs) with 2-fold interpenetrated pillared layer structure formulated as $\{[Co_2(BTTB)\cdot(BPY)]\cdot(H_2O)(DEF)_2\}_n$ (**3**), $\{[Zn_2(BTTB)\cdot(BPY)]\cdot(DEF)_2\}_n$ (**4**), $\{[Co_2(BTTB)\cdot(AZPY))]\cdot(DEF)_2\}_n$ (**5**) and $\{[Zn_2(BTTB)\cdot(AZPY))]\cdot(DEF)_2\}_n$ (**6**) have been synthesized (H_4BTTB = 4,4',4",4'"-benzene-1,2,4,5-tetrayltetrabenzoic acid, BPY = 4,4'-bipyridine, AZPY = 4,4'-azopyridine). In all these MOFs, $\{M_2(O_2CR)_4\}$ paddlewheel units are connected by $BTTB^{4-}$ ligands to form a layer which is further pillared together by BPY or AZPY linkers, giving rise to a porous 3D framework. Two individual 3D frameworks interpenetrate with each other forming the final structure of this series of MOFs. All these four MOFs demonstrate good thermal stability and permanent porosity and their structures have been determined by single crystal X-ray diffraction analyses and further characterized by PXRD, thermo gravimetric analyses, and nitrogen adsorption at 77 K.

The designing of a pillared three-dimensional (3-D) MOF involves using an appropriate bridging linker to act as a pillar to connect with well-defined two-dimensional (2D) grid sheets formed from paddle wheel clusters $M_2(COO)_4$ as nodes and bicarboxylates or tetracarboxylate ligands (Scheme S1). The pores within pillared 3D MOFs are predetermined by the different combinations of carboxylate ligands and pillar linkers. The pillared layer approach in combination with interpenetration strategy (as shown in Figure 1), can guide the realization of small micropores and help in tuning for use in highly selective separation and purification of small molecules.[1] Furthermore, this approach enhances the stability of the ultimate framework and makes it easier to obtain the targeted product.[2]

In this work, we have chosen H_4BTTB as carboxylate linker and BPY and AZPY (Scheme S2) as pillars for the construction of paddle wheel type MOFs. We have chosen BTTB as the carboxylate linker due to the following reasons: a) they contain four potential metal binding sites, which can yield the formation of a MOF through multiple bonding interactions; b) its rigidness can enable the preparation of permanently porous materials; c) its long molecular structure can give rise to the formation of microporous coordination frameworks through framework interpenetration; (d) there are only a few reports of MOFs[3] containing this carboxylic acid.

BPY and AZPY were chosen as pillars as they are widely used for the construction of pillared type of MOFs. They can act as a rigid pillared building block to form robust MOFs with metal ions and the axial nitrogen atoms can participate in coordination bonding and can play an important role in the assembly of MOFs. Furthermore, in the case of AZPY ligand, the free basic nitrogen centers might potentially serve as the primary adsorption sites.[4]

Experimental Section

Materials and methods. All commercially available chemicals and solvents are of reagent grade and were used as received without further purification. Thermogravimetric analyses (TGA) were carried out in the temperature range of 25-700 ˚C on a NETSZCH TG/Mass spectrometry analyzer under helium with a heating rate of 5 ˚C/min. Powder X-ray diffraction patterns (PXRD) were recorded on a X'Pert X-ray PANalytical diffractometer with an X'accelerator module using Cu Kα (λ = 1.5418 Å) radiation at room temperature, with a step size of 0.02˚ in 2θ. Nitrogen (N_2) adsorption isotherms were measured at 77 K with an Autosorb 1-MP from Quantachrome Instruments. CCDC 986374-986376 contain the supplementary crystallographic data for **3**, **4**, and **5**.

Synthesis of MOFs.

$\{[Co_2(BTTB)\cdot(BPY)]\cdot(H_2O)(DEF)_2\}_n$ (3). A mixture of $Co(NO_3)_2\cdot 6H_2O$ (58.2 mg, 0.2 mmol), H_4BTTB (55.8 mg, 0.1 mmol), and BPY (15.6 mg, 0.1 mmol) was dissolved in 5 mL of DEF/ethanol/water (2:2:1, v/v). Two drops of 1N HCl was added to the mixture, and the final mixture was placed in a Parr Teflon-lined stainless steel container under autogenous pressure and heated at 100 ˚C for 4 days. Large quantities of purple-block crystals (Figure S18) were obtained. The crystals were filtered out, washed with mother liquid, and dried at ambient conditions. Elemental analysis (%) calcd: C 61.6 H 5.16 N 5.32 Found: C 61.99 H 5.07 N 5.19. Yield: 79 mg (75%, based on Co).

$\{[Zn_2(BTTB)\cdot(BPY)]\cdot(DEF)_2\}_n$ (4). A mixture containing $Zn(NO_3)_2\cdot 6H_2O$ (59.4 mg, 0.2 mmol), H_4BTTB (55.8 mg, 0.1 mmol), 2 mL DEF, 2 mL ethanol, 1 mL water, and 2 drops of 1N HCl was sealed in a 23 mL Teflon lined stainless steel container and heated at 100 ˚C for 4 days. After cooling to room temperature, colorless block shaped crystals of **1** were obtained (Figure S19). Elemental analysis (%) Calcd : C: 53.92 H 5.44 N 3.85 Found: C 54.57 H 4.92 N

3.2. Yield: 58.1 mg (27% based on Zn).

{[Co_2(BTTB)·(AZPY))]·$(DEF)_2$}$_n$ (5). A mixture of $Co(NO_3)_2·6H_2O$ (43.6 mg, 0.2 mmol), H_4BTTB (55.8 mg, 0.1 mmol), and AZPY (18.4 mg, 0.1 mmol) was dissolved in 5 mL of DEF/ethanol/water (2:2:1,v/v). Two drops of 1N HCl was added to the mixture, and the final mixture was placed in a Parr Teflon-lined stainless steel container under autogenous pressure and heated at 100 ˚C for 4 days. Large quantities of red plate crystals (Figure S20) were obtained. The crystals were filtered off, washed with mother liquid, and dried at ambient conditions. Elemental analysis (%) calcd: C 61.34 H 5.04 N 7.80 Found: C 59.11 H 4.93 N 7.08. Yield: 82.7 mg (76.79 % based on Co).

{[Zn_2(BTTB)·(AZPY))]·$(DEF)_2$}$_n$ (6). A mixture of $Zn(NO_3)_2·6H_2O$ (59.4 mg, 0.2 mmol), H_4BTTB (55.8 mg, 0.1 mmol), and AZPY (18.4 mg, 0.1 mmol) was dissolved in 5 mL of DEF/ethanol/water (2:2:1,v/v). Two drops of 1N HCl was added to the mixture, and the final mixture was placed in a Parr Teflon-lined stainless steel container under autogenous pressure and heated at 100 ˚C for 4 days. Large quantities of orange plate crystals (Figure S21) were obtained. The crystals were filtered off, washed with mother liquid, and dried at ambient conditions. Elemental analysis (%) calcd : C 60.61 H 4.99 N 7.71 Found: C 59.48 H 5.38 N 7.87. Yield: 83.4 mg (76.5 % based on Zn).

X-ray crystallography. All single crystal data were collected on a Bruker SMART APEX CCD sealed tube diffractometer by using Mo-*K*α radiation with a graphite monochromator. Crystals of the MOFs were mounted on nylon CryoLoops with Paratone-N. The structure was solved by direct methods and refined on F^2 by full-matrix least-squares using the SHELXTL-97 software suite. Anisotropic thermal parameters were refined for all non-hydrogen atoms; hydrogen atoms were refined isotropically as riding atoms. Some of the hydrogen atoms could not be resolved, and thus were not included in the analysis. The guest molecules inside the pores could not be refined owing to severe disorder, as common to microporous MOFs. For all the compounds, the routine SQUEEZE in PLATON was used to remove the very diffuse electron density associated with the disordered solvent molecules in the pores.[5] For **CoBTTBBPY**, we refined the structure using twinning mode. For **ZnBTTBBPY**, we treated both BTTB and BPY ligand in disordered model. To determine the occupancy of the disordered part of BPY ligand, firstly we refined C14A C14B C15A C15B freely and found that the occupancy is about 0.15, 0.35, 0.15, 0.35 respectively, then

we refined the structure by fixing the occupancy to be 0.15, 0.35, 0.15, 0.35, respectively. For **CoBTTBAZPY**, we treated AZPY ligand in the structure as disordered and some restrains were made on it. Pertinent crystallographic data and structure refinement data are summarized in Table S1.

Structural description

{[Zn_2(BTTB)·(BPY)]·$(DEF)_2$}$_n$ (4). The structures of compound **3** and compound **4** are identical, thus only compound **4** is described. Single-crystal X-ray structural analysis showed that compound **4** crystallizes in the space group of *Imma*. The asymmetric unit contains two one-fourth Zn^{2+} ions, one-fourth BTTB ligand and one-fourth BPY ligand. Both Zn1 and Zn2 show the same square pyramidal coordination geometry, with four oxygen atoms from four different BTTB ligands occupying the equatorial plane and one nitrogen atom from BPY ligand occupying the axial position (Figure S4). The average Zn-O and Zn-N bond lengths are 2.026 Å and 2.05 Å, respectively. Four carboxylate groups bridge two Zn^{2+} ions, giving rise to a well-known {$Zn_2(O_2CR)_4$} paddlewheel second building unit (SBU) with Zn-Zn distance of 2.727 Å (Figure S4). These paddlewheel units are further connected by $BTTB^{4-}$ ligands to form a square grid layer (Figure S1a), which is further pillared by BPY linkers resulting in a 3D porous framework with channels along [1 0 0], [0 1 0], [0 0 1] and [0 -1 1] directions (Figure S1b). Two individual frameworks interpenetrated with each other, leading to the channels along [1 0 0] and [0 0 1] directions are blocked, leaving the channels along [0 1 0] and [0 -1 1] directions with sizes of 4.064 Å and 6.044 Å, respectively (Figure S1c). As estimated by PLATON[5], the solvent accessible volume in compound **2** is 39.2% of total unit cell volume.

{[Co_2(BTTB)·(AZPY))]·$(DEF)_2$}$_n$ (5). The structures of compound **5** and compound **6** are identical and isostructural to compound **4**, thus only compound **5** is briefly described. Compound **5** crystallizes in the triclinic space group *P-1* and the asymmetric unit contains two Co^{2+} ions, one BTTB ligand and one APY ligand. The Co^{2+} ions show the same square pyramidal coordination geometry to the Zn^{2+} ions in compound **4** (Figure S5). As compound **4**, the {$Co_2(O_2CR)_4$} paddlewheel second building units are connected by $BTTB^{4-}$ ligands to form a square grid layer. Different from compound **4**, these square grid layers are further pillared by APY linker instead of BPY linker to form a 3D porous framework (Figure S2a). Two individual frameworks

interpenetrated with each other to form the final structure with channels along [1 0 0], [-1, 1, 1], [1 0 1] directions with sizes of 4.942 Å, 4.942 Å, 6.617 Å, respectively (Figure S2b). As estimated by PLATON[5], the solvent accessible volume in compound **5** is 39.4% of total unit cell volume.

Surface area, bulk phase purity and thermal properties

After the synthesis, all MOFs synthesized in this work were solvent exchanged with chloroform and activated at 120 ˚C overnight under vacuum. BET surface areas were measured after each activation process. The properties of MOFs synthesized in this work along with the BET surface areas and predicted accessible surface areas[6] are shown in Table S2. The experimental BET surface areas are only half of that calculated geometrically from the perfect crystal structure with nitrogen molecule as a probe.[6] This discrepancy can be attributed to the crystal defects present in the experimental samples. The presence of trapped solvent molecules in the crystals can be ruled out here as thermogravimetric measurements showed complete removal of solvent molecules.

The N_2 adsorption/desorption isotherms measured at 77 K for compounds **3**, **4**, **5** and **6** (Figures S6-S9) reveals typical type-I behavior, as expected for microporous materials. Fitting the Brunauer-Emmett-Teller (BET) equation to their respective N_2 adsorption isotherms within the range $0.007<P/P_0<0.03$ gives an estimated surface area of 843 m^2/g for **3**, 841 m^2/g for **4**, 805 m^2/g for **5**, and 647 m^2/g for **6**, respectively. The Dubinin-Astakhov (DA) equation gives an estimated pore volume of 0.396 cm^3/g for **3**, 0.38 cm^3/g for **4**, 0.389 cm^3/g for **5**, and 0.357 cm^3/g for **6**, respectively.

In order to confirm the phase purity of the bulk materials **3**, **4**, **5**, and **6**, PXRD experiments were carried out. The PXRD experimental and simulated patterns for each MOF are shown in Figures S3 and Figures S10 – S13. Note that, single-crystal X-ray data for **6** was not obtained. Therefore, their experimental PXRD patterns were compared to the simulated patterns of **5**. Figure S10 shows that **3** and **4** are isostructural while Figure S12 shows that **5** and **6** are isostructural. Figure S3a and Figure S11 show that the as-synthesized and activated frameworks of **3** and **4** have PXRD patterns that are coincident with the corresponding patterns simulated from single-crystal XRD structures. Figure S3b shows that all the peaks of activated **6** matches well with the corresponding patterns simulated from single-crystal XRD structure of **5**, while for the as-synthesized sample of **6** and the activated, chloroform exchanged and the as-synthesized samples of **5** (Figure S13), only the major

peaks of their PXRD patterns match well with that of simulated pattern. The minor peaks at 10˚, 11˚, however do not appear in their PXRD patterns. All compounds **3, 4, 5,** and **6** are stable in air and insoluble in water, and most of the common organic solvents such as chloroform, methanol, acetone, toluene, and dimethyl formamide.

Thermogravimetric data of all MOFs synthesized in this work are shown in Figures S14-S17. **3** displays a thermal stability of ~ 450 ˚C (Figure S14). A two-step steady weight loss of ~ 18%, corresponding to removal of uncoordinated solvent molecules is seen between room temperature and 250 ˚C and a rapid weight loss beyond 500 ˚C suggests the framework breakdown due to the decomposition of BTTB ligand. Guest molecules were solvent exchanged with chloroform and removal of guest molecules in **3** was done at 120 ˚C for 12 hr under vacuum and this was confirmed from the thermogravimetric data and PXRD data of activated sample of **3**.

The TGA curve of **4** (Figure S15) shows that initial weight loss begins at 100 ˚C and continues till 250 ˚C and then reaches a plateau. The total weight loss over this range is ~18 % which corresponds to loss of most of the coordinated and uncoordinated solvent molecules. This compound has a thermal stability of 350 ˚C. Beyond this temperature, it undergoes a rapid weight loss that can be attributed to the decomposition of organic linkers. Removal of guest molecules from **4** was done with chloroform exchange and activation at 120 ˚C for 12 hrs under vacuum and this was confirmed from the thermogravimetric data and PXRD data of activated sample of **4**.

Compound **5** undergoes a steady weight loss of ~ 18 % of uncoordinated solvent molecules from 120 ˚C to 250 ˚C and reaches a small region of plateau from 250 to 300 ˚C (Figure S16). Removal of guest molecules from **5** was done with chloroform exchange and activation at 120 ˚C for 12 hr under vacuum and this was confirmed from the thermogravimetric data and PXRD data of activated sample of **5**.

Compound **6** undergoes a steady weight loss of ~ 18 %, from 120 to 250 ˚C and then reaches a small region of plateau and beyond 325 ˚C, a rapid weight loss occurs (Figure S17). The weight loss of ~ 18 % corresponds to removal of uncoordinated solvent molecules. Removal of guest molecules from **6** was done with chloroform exchange and activation at 120 ˚C for 12 hr under vacuum and this was confirmed from the thermogravimetric data and PXRD data of activated sample of **6**.

REFERENCES

(1) Chen, B. L.; Ma, S. Q.; Zapata, F.; Fronczek, F. R.; Lobkovsky, E. B.; Zhou, H. C. *Inorg. Chem.* **2007**, *46*, 1233.

(2) Du, X. D.; Xiao, H. P.; Zhou, X. H.; Wu, T.; You, X. Z. *J. Solid State Chem.* **2010**, *183*, 1464.

(3) Farha, O. K.; Malliakas, C. D.; Kanatzidis, M. G.; Hupp, J. T. *J. Am. Chem. Soc.* **2010**, *132*, 950.

(4) Zelenak, V.; Vargova, Z.; Almasi, M.; Zelenakova, A.; Kuchar, J. *Micropor. Mesopor. Mater.* **2010**, *129*, 354.

(5) Spek, A.L. **2005**, PLATON, A Multipurpose Crystallographic Tool, Utrecht University, Utrecht, The Netherlands.

(6) Duren, T.; Millange, F.; Frey, G.; Walton, K. S.; Snurr, R. Q. *J. Phys. Chem. C* **2007**, *111*, 15350.

Table S1. Crystallographic data for compounds **3-5**

Compound	**3**	**4**	**5**
Formula	$C_{22}H_{13}CoNO_4$	$C_{22}H_8NO_4Zn$	$C_{44}H_{26}Co_2N_4O_8$
*F*w	417.18	415.66	856.52
Crystal size(mm)	0.10 × 0.12 × 0.08	0.12 × 0.10 × 0.10	0.10 × 0.10 × 0.08
Space group	*Imma*	*Imma*	*P-1*
a(Å)	31.02(5)	30.947(8)	11.761(5)
b(Å)	11.74(2)	11.625(3)	15.417(6)
c(Å)	13.91(3)	13.967(4)	15.705(6)
$\alpha(^o)$	90	90	98.664(6)
$\beta(^o)$	90	90	103.082(6)
$\gamma(^o)$	90	90	90.032(6)
$V(Å^3)$	5066(16)	5025(2)	2740.3(19)
Z	8	8	2
$\lambda(K\alpha)$(Å)	0.71073	0.71073	0.71073
$D_c(g/cm^3)$	1.060	1.099	1.033
$\mu(mm^{-1})$	0.697	0.998	0.648
T(K)	296(2)	296(2)	173(2)
Total reflections	33881	46289	36659
Unique data collected	2494	3691	9699
Observed reflections	2210	3189	6312
*R*int	0.0621	0.0706	0.0703
Parameters	186	190	533
R_1, *w*R(I > 2σ(I))[a]	0.1007, 0.2528	0.0639, 0.1667	0.0804, 0.2314
R_1, *w*R(all data)[b]	0.1058, 0.2572	0.0727, 0.1724	0.1009, 0.2432
$w=1/[\sigma^2(F_0^2)+(aP)^2+bp]$	a = 0.1588, b = 40.8245	a = 0.0863, b = 28.6375	a = 0.1601, b = 0.0000
Goodness-of-fit-on F^2	1.062	1.069	1.016
$\Delta\rho_{min}$ and $\Delta\rho_{max}$(e $Å^{-3}$)	-1.570, 6.754	-1.112, 4.830	-1.112, 1.160

[a] $R = \sum||F_0|-|F_c||)/\sum|F_0|$

[b] $wR = |\sum w(F_0-F_c)^2/\sum w(F_0^2)^2|^{1/2}$

Table S2. Properties and thermal treatment conditions for Compounds **3-6**

MOF	Pore size (Å)	Pore volume (cm^3/g)	BET surface area (m^2/g)	Activation process (under vacuum)	Thermal stability	Features	Calculated Accessible Surface Area (m^2/g)
3	4.064	0.396	843	Chloroform Exchange and 120 ˚C (12 h)	400 ˚C	2-D pore system, interpenetrated	-
4	4.064	0.38	841	Chloroform Exchange and 120 ˚C (12 h)	350 ˚C	2-D pore system, interpenetrated	1660
5	4.942	0.389	805	Chloroform Exchange and 120 ˚C (12 h)	300 ˚C	3-D pore system, interpenetrated	2038
6	4.942	0.357	647	Chloroform Exchange and 120 ˚C (12 h)	300˚C	3-D pore system, interpenetrated	-

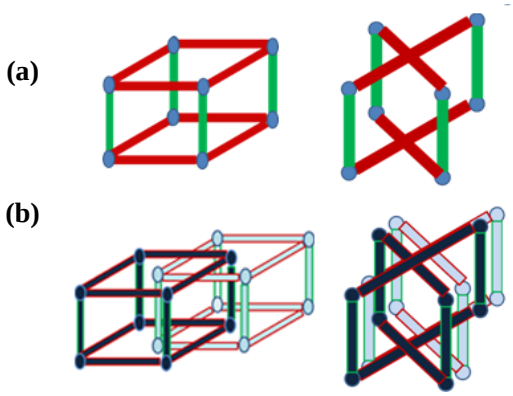

Scheme S1. a) Cartoon representation of formation of pillared layer frameworks from bicarboxylate ligand (top left) and tetracarboxylate ligand (top right) pillared by dipyridyl strut (green). The blue corners are the cobalt or copper or zinc paddlewheel nodes. b) Interpenetrated pillared layer frameworks from bicarboxylate ligand (bottom left) and tetracarboxylate ligand (bottom right). Light blue and dark blue represents different frameworks.

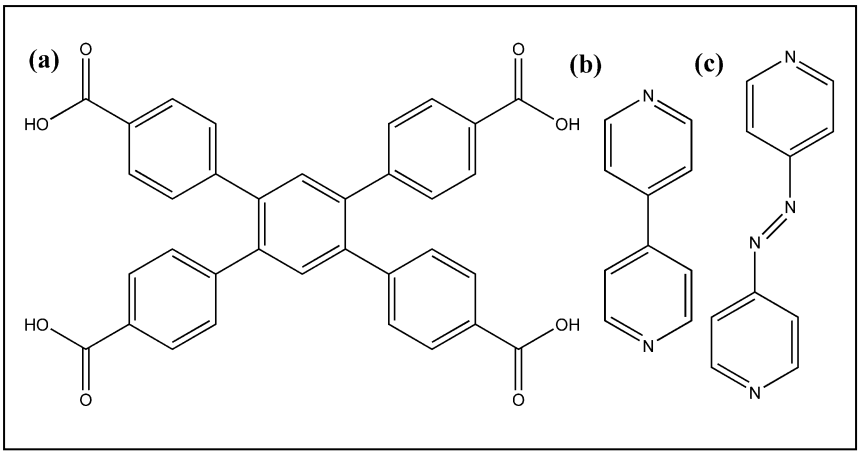

Scheme S2. Organic ligands a) H_4BTTB, b) BPY, c) AZPY employed in this work

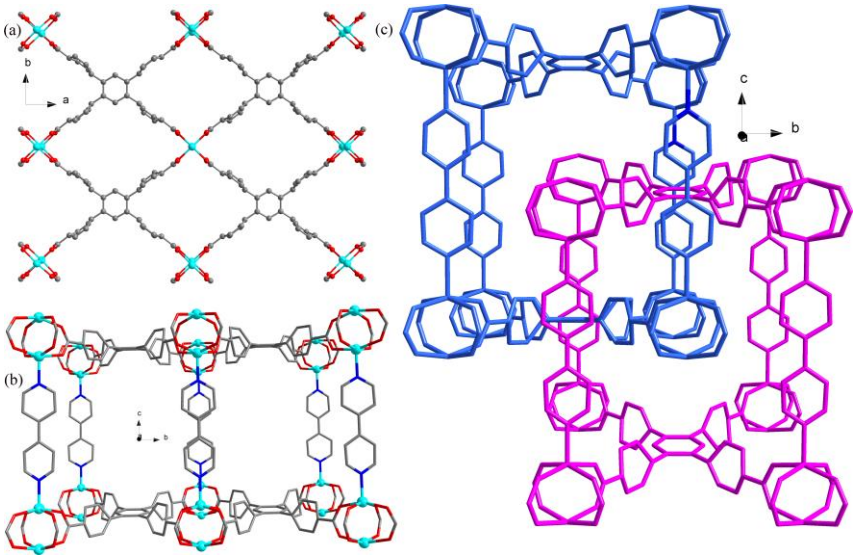

Figure S1. a) The square grid layer constructed by paddlewheel SBUs in compound **4**. b) The 3D porous pillared layer framework of compound **4**. c) The interpenetrated pillared layer frameworks of compound **4**.

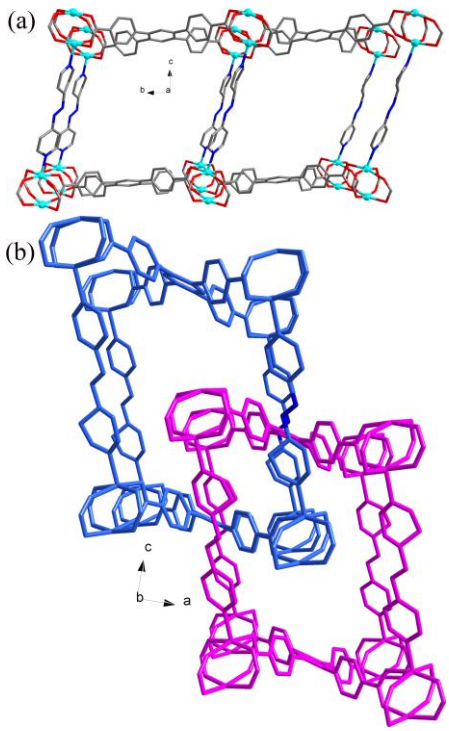

Figure S2. a) The 3D porous pillared layer framework of compound **5**. b) The interpenetrated pillared layer frameworks of compound **5**.

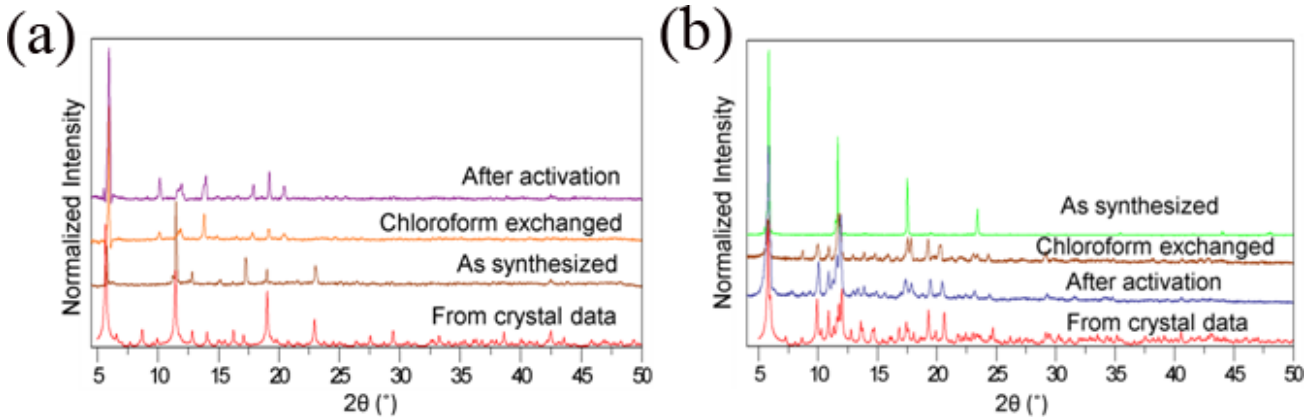

Figure S3. Simulated, as synthesized, chloroform exchange and activated powder X-ray diffraction patterns of **4** a) and of **6** b).

***Table S3*. Selected bond lengths [Å] and angles [°] for 3.**

Compound **3** (bond)			
Co1—O1^{i}	2.009 (7)	Co2—O2^{iii}	2.044 (6)
Co1—O1^{ii}	2.009 (7)	Co2—O2	2.044 (5)
Co1—O1^{iii}	2.009 (7)	Co2—O2^{i}	2.044 (6)
Co1—O1	2.009 (7)	Co2—O2^{ii}	2.044 (5)
Co1—N2^{iv}	2.063 (13)	Co2—N1	2.049 (12)
Co1—Co2	2.727 (6)		
(angle)			
O1^{i}—Co1—O1^{ii}	88.0 (5)	O2^{iii}—Co2—O2	90.6 (4)
O1^{i}—Co1—O1^{iii}	90.2 (5)	O2^{iii}—Co2—O2^{i}	87.4 (4)
O1^{ii}—Co1—O1^{iii}	165.6 (3)	O2—Co2—O2^{i}	164.7 (3)
O1^{i}—Co1—O1	165.6 (3)	O2^{iii}—Co2—O2^{ii}	164.7 (3)
O1^{ii}—Co1—O1	90.2 (5)	O2—Co2—O2^{ii}	87.4 (4)
O1^{iii}—Co1—O1	88.0 (5)	O2^{i}—Co2—O2^{ii}	90.6 (4)
O1^{i}—Co1—N2^{iv}	97.21 (17)	O2^{iii}—Co2—N1	97.66 (17)
O1^{ii}—Co1—N2^{iv}	97.21 (17)	O2—Co2—N1	97.66 (17)
O1^{iii}—Co1—N2^{iv}	97.21 (17)	O2^{i}—Co2—N1	97.66 (17)
O1—Co1—N2^{iv}	97.21 (17)	O2^{ii}—Co2—N1	97.66 (17)

Symmetry codes: (i) 1-x, 1/2-y, z; (ii) x, y, 1+z; (iii) 1+x, 1+y, z; (iv) x, y, 1+z.

***Table S4*. Selected bond lengths [Å] and angles [°] for 4.**

Compound **4** (bond)			
Zn1—O1^{i}	1.993 (10)	Zn2—N1	2.033 (10)
Zn1—O1^{ii}	1.993 (10)	Zn2—O2^{ii}	2.050 (5)
Zn1—O1^{iii}	1.993 (10)	Zn2—O2^{i}	2.050 (5)
Zn1—O1	1.993 (10)	Zn2—O2^{iii}	2.050 (5)
Zn1—N2^{iv}	2.018 (11)	Zn2—O2	2.050 (5)
Zn1—Zn2	2.8939 (19)		
(angle)			
O1^{i}—Zn1—O1^{ii}	158.4 (5)	N1—Zn2—O2^{ii}	99.99 (16)
O1^{i}—Zn1—O1^{iii}	91.8 (6)	N1—Zn2—O2^{i}	99.99 (16)
O1^{ii}—Zn1—O1^{iii}	84.2 (6)	O2^{ii}—Zn2—O2^{i}	160.0 (3)
O1^{i}—Zn1—O1	84.2 (6)	N1—Zn2—O2^{iii}	99.99 (16)
O1^{ii}—Zn1—O1	91.8 (6)	O2^{ii}—Zn2—O2^{iii}	87.1 (3)
O1^{iii}—Zn1—O1	158.4 (5)	O2^{i}—Zn2—O2^{iii}	89.5 (3)
O1^{i}—Zn1—N2^{iv}	100.8 (3)	N1—Zn2—O2	99.99 (16)
O1^{ii}—Zn1—N2^{iv}	100.8 (3)	O2^{ii}—Zn2—O2	89.5 (3)
O1^{iii}—Zn1—N2^{iv}	100.8 (3)	O2^{i}—Zn2—O2	87.1 (3)
O1—Zn1—N2^{iv}	100.8 (3)	O2^{iii}—Zn2—O2	160.0 (3)

Symmetry codes: (i) x, y, 1+z; (ii) 1+x, 1+y, z; (iii) 1-x, 1/2-y, z; (iv) x, y, 1+z.

***Table S5*. Selected bond lengths [Å] and angles [°] for 5.**

Compound **5** (bond)			
Co1—O8^{i}	2.014 (2)	Co2—O3^{ii}	2.015 (2)
Co1—O2	2.023 (2)	Co2—O7^{i}	2.024 (2)
Co1—O4^{ii}	2.036 (2)	Co2—O5^{iii}	2.044 (2)
Co1—N1	2.064 (2)	Co2—N2^{iv}	2.077 (2)
Co1—O6^{iii}	2.126 (2)	Co2—O1	2.109 (2)
Co1—Co2	2.7873 (6)		
(angle)			
O8^{i}—Co1—O2	97.99 (10)	O3^{ii}—Co2—O7^{i}	165.79 (9)
O8^{i}—Co1—O4^{ii}	162.79 (9)	O3^{ii}—Co2—O5^{iii}	96.91 (10)
O2—Co1—O4^{ii}	89.18 (10)	O7^{i}—Co2—O5^{iii}	87.77 (10)
O8^{i}—Co1—N1	98.38 (10)	O3^{ii}—Co2—N2^{iv}	95.89 (10)
O2—Co1—N1	103.61 (10)	O7^{i}—Co2—N2^{iv}	95.84 (10)
O4^{ii}—Co1—N1	95.06 (10)	O5^{iii}—Co2—N2^{iv}	105.00 (10)
O8^{i}—Co1—O6^{iii}	85.43 (9)	O3^{ii}—Co2—O1	86.07 (10)
O2—Co1—O6^{iii}	164.07 (10)	O7^{i}—Co2—O1	85.73 (10)
O4^{ii}—Co1—O6^{iii}	83.59 (10)	O5^{iii}—Co2—O1	163.23 (10)
N1—Co1—O6^{iii}	91.19 (11)	N2^{iv}—Co2—O1	91.04 (10)

Symmetry codes: (i) x, 1+y, z; (ii) 1+x, y, z; (iii) 1+x, 1+y, z; (iv) x, y, 1+z.

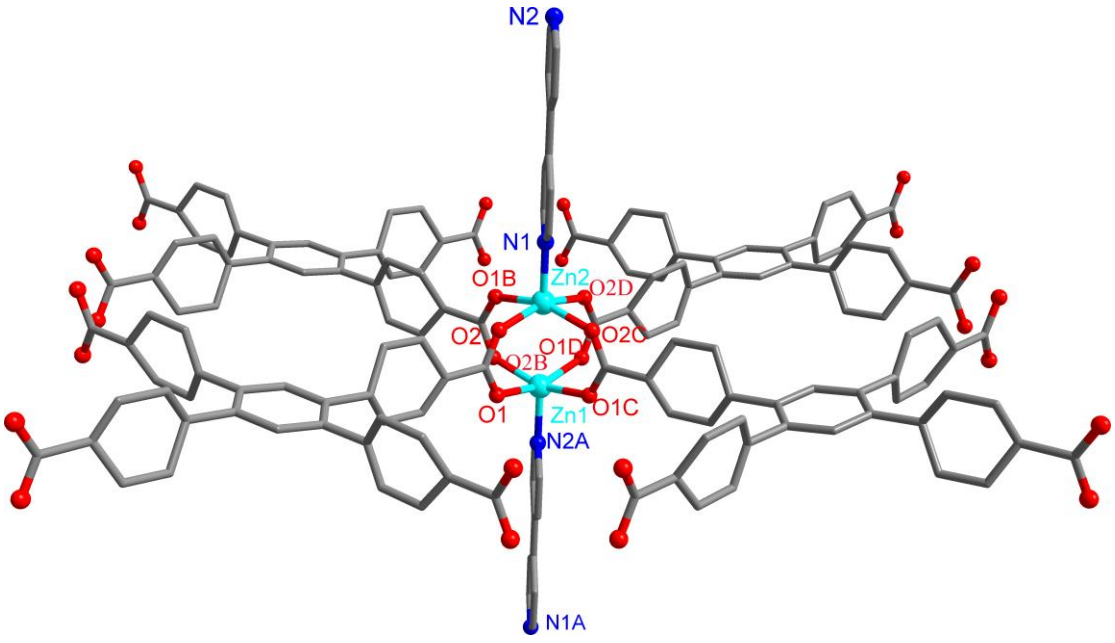

Figure S4. Coordination environment of Zn^{2+} ions in compound **4** Symmetry codes: (A) x, y, 1+z; (B) x, 1/2-y, -z; (C) 1-x, y, z; (D)1-x, 1/2-y, z.

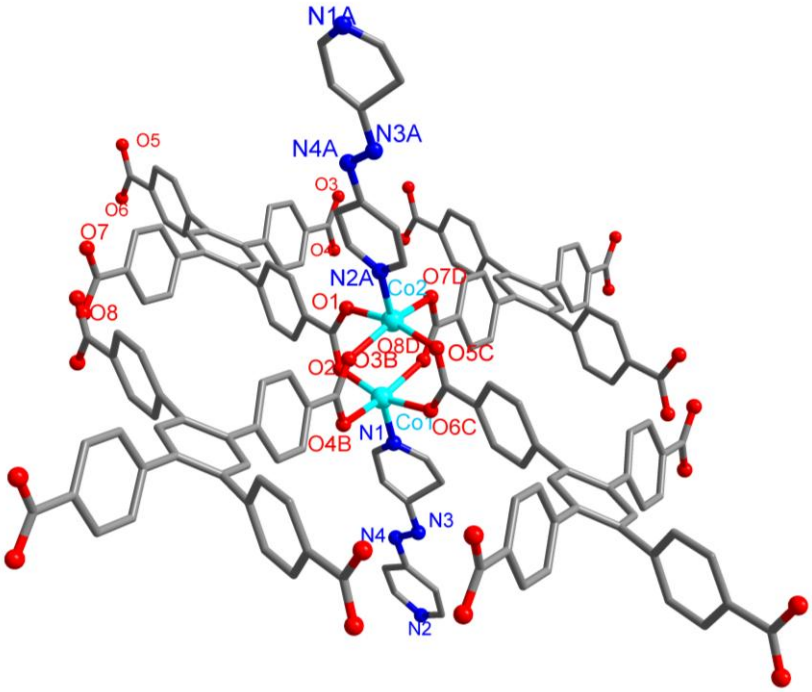

Figure S5. Coordination environment of Co^{2+} ions in compound **5** Symmetry codes: (A) x, y, 1+z; (B) 1+x, y, z; (C)1+ x, 1+y, z; (D) x, 1+y, z.

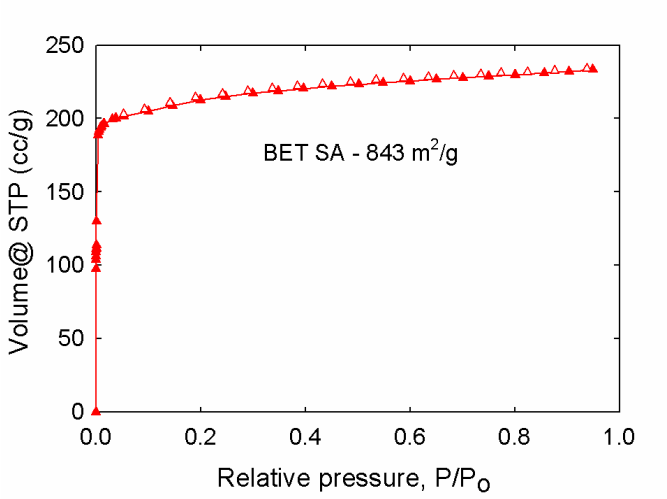

Figure S6. Nitrogen isotherm of activated **3** at 77 K (closed symbols – adsorption, open symbols – desorption).

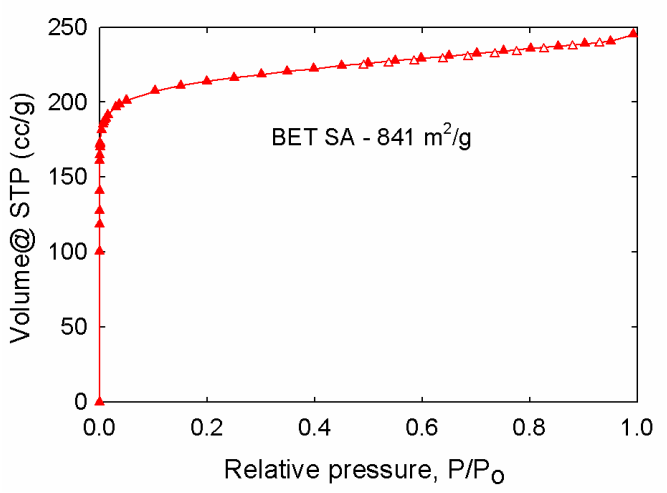

Figure S7. Nitrogen isotherm of activated **4** at 77 K (closed symbols – adsorption, open symbols – desorption).

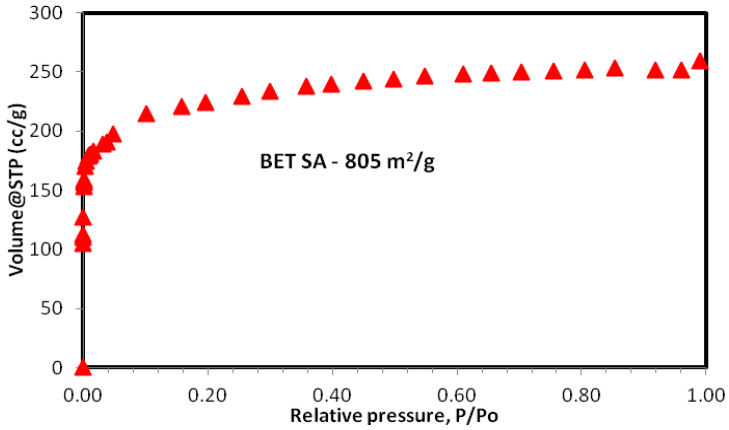

Figure S8. Nitrogen isotherm of activated **5** at 77 K (closed symbols – adsorption, desorption data is not reported since liquid nitrogen levels were not maintained well enough during the desorption runs)

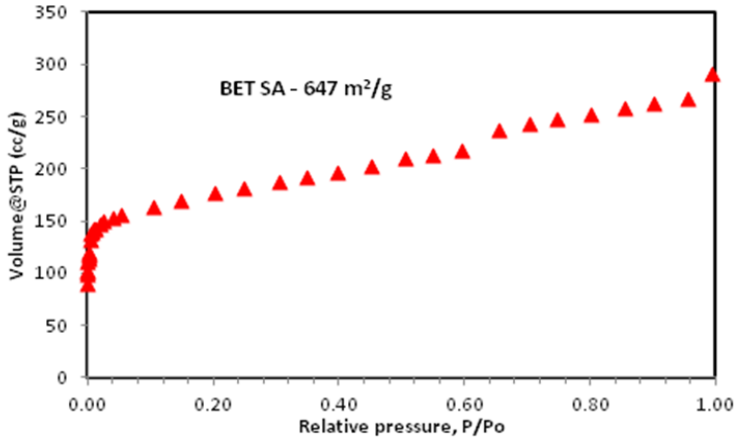

Figure S9. Nitrogen isotherm of activated **6** at 77 K (closed symbols – adsorption, desorption data is not reported since liquid nitrogen levels were not maintained well enough during the desorption runs)

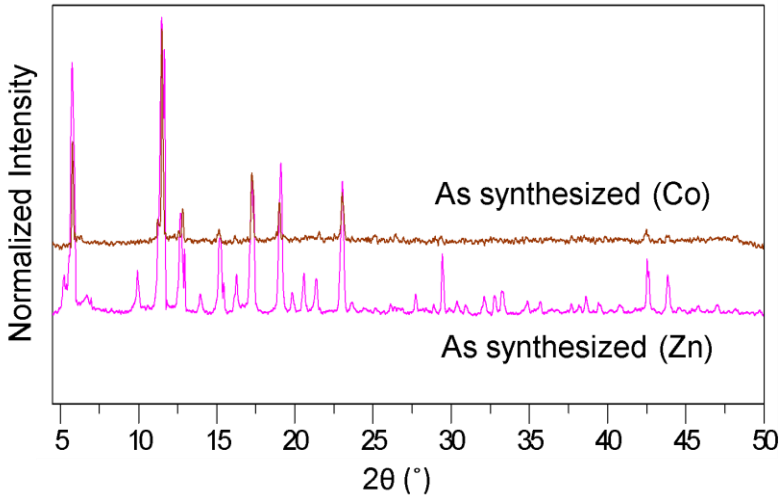

Figure S10. As synthesized powder X-ray diffraction patterns of **3** and **4**

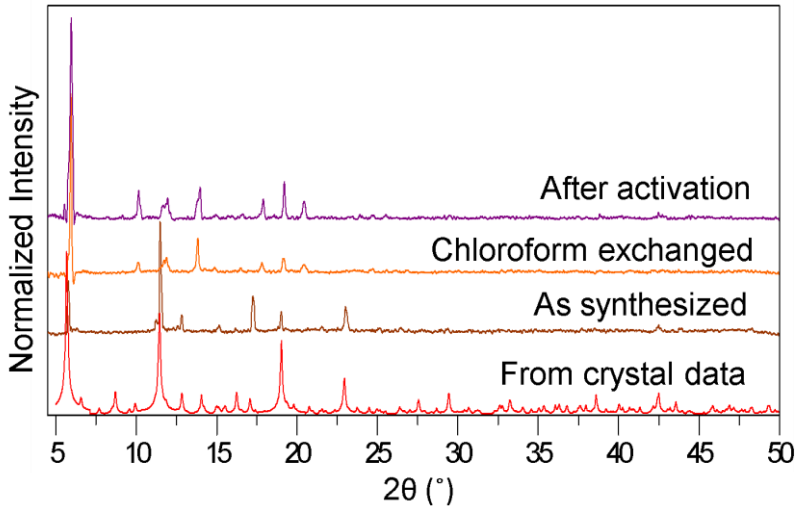

Figure S11. Simulated, as synthesized, chloroform exchanged and activated powder X-ray diffraction patterns of **3**

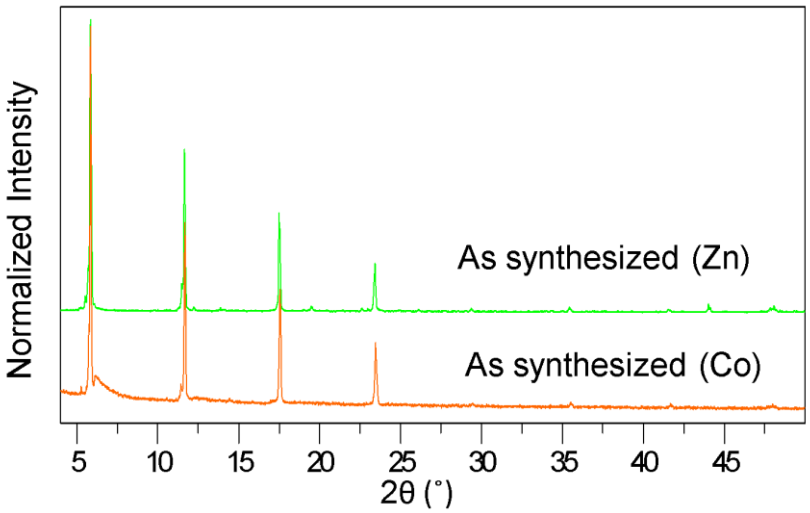

Figure S12. As synthesized powder X-ray diffraction patterns of **5** and **6**

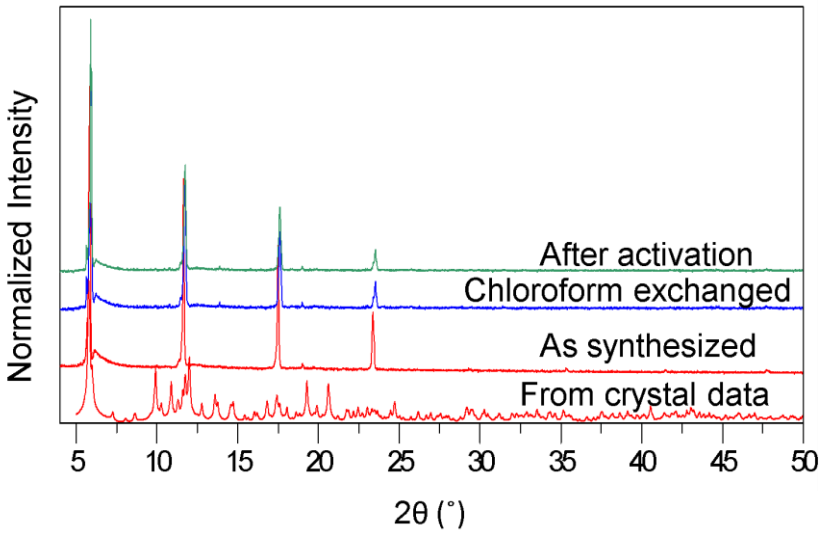

Figure S13. Simulated, as-synthesized, chloroform exchanged and activated powder X-ray diffraction patterns of **5**

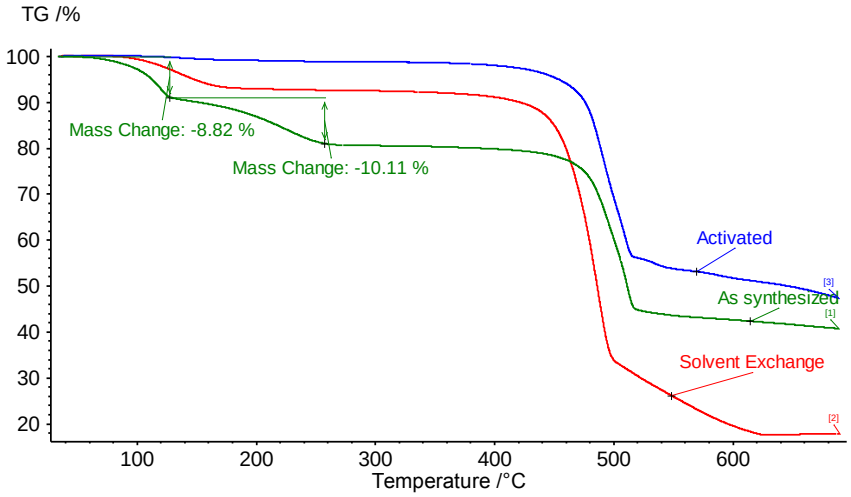

Figure S14. TGA trace of **3**.

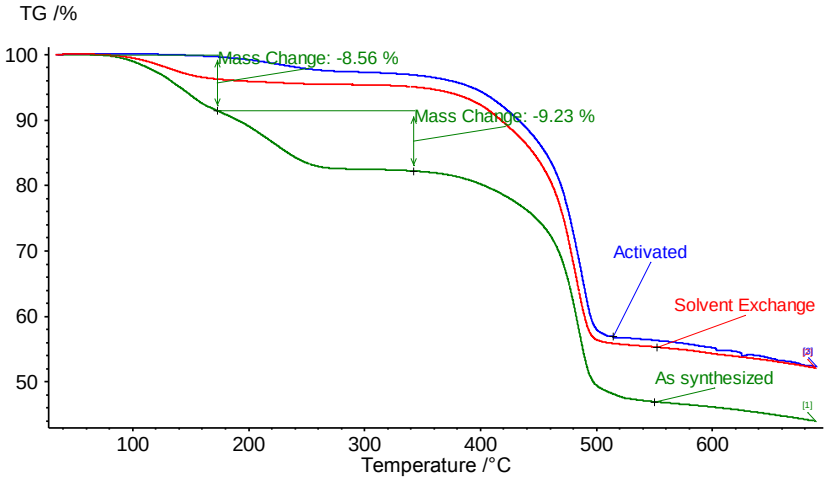

Figure S15. TGA trace of **4**.

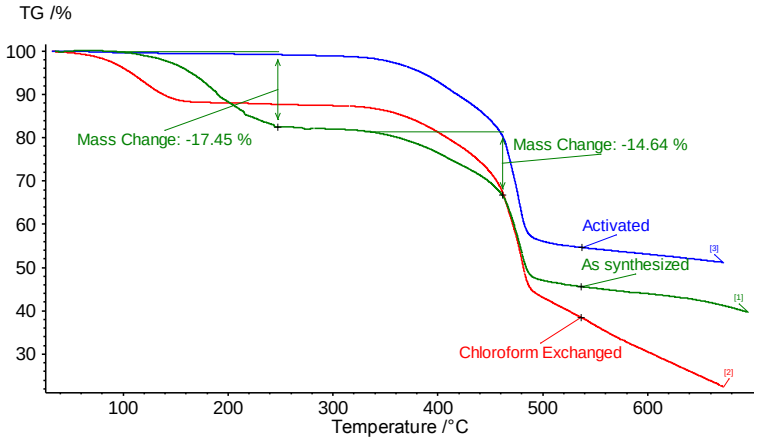

Figure S16. TGA trace of **5**.

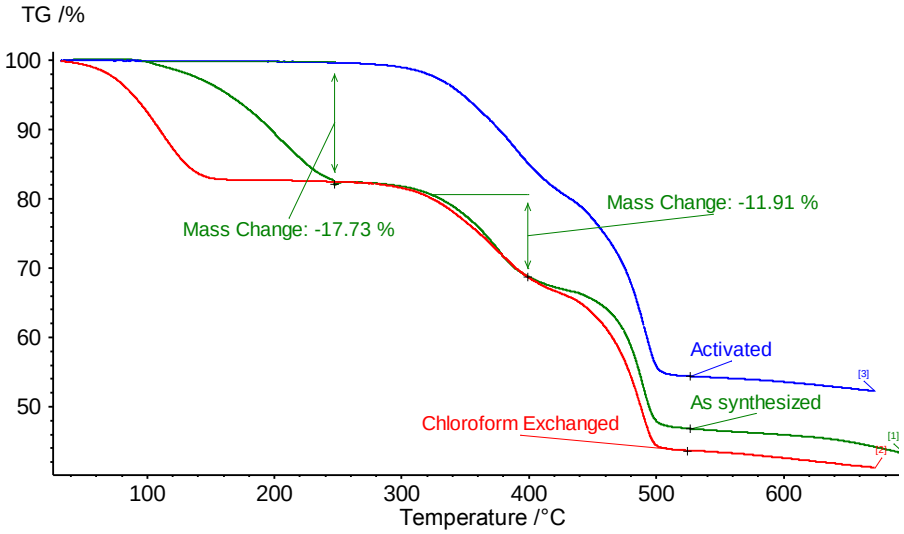

Figure S17. TGA trace of **6**.

.

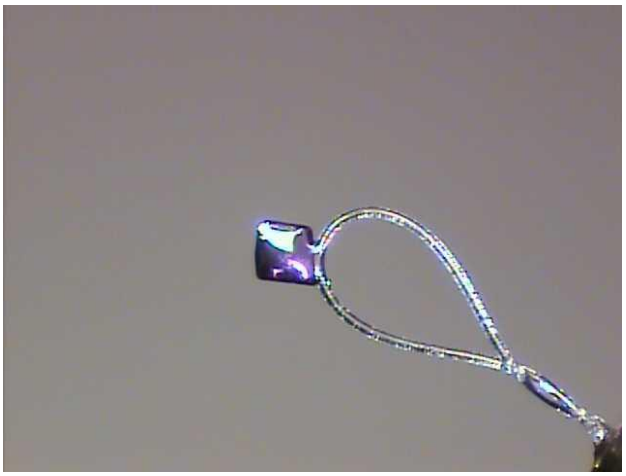

Figure S18. Photograph of single crystal of **3** (size (mm) – 0.1 x 0.12 x 0.08)

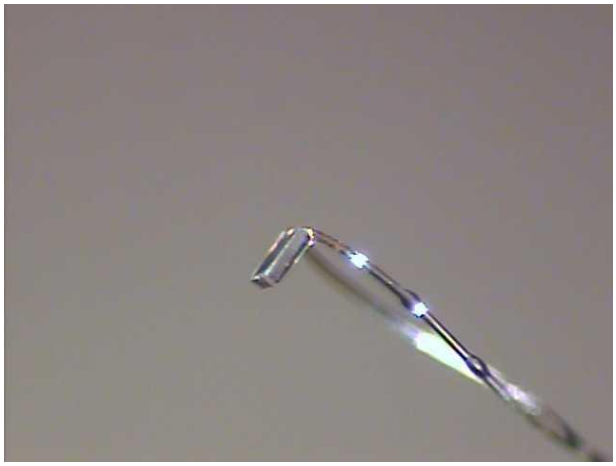

Figure S19. Photograph of single crystal of **4** (size (mm) – 0.12 x 0.1 x 0.1)

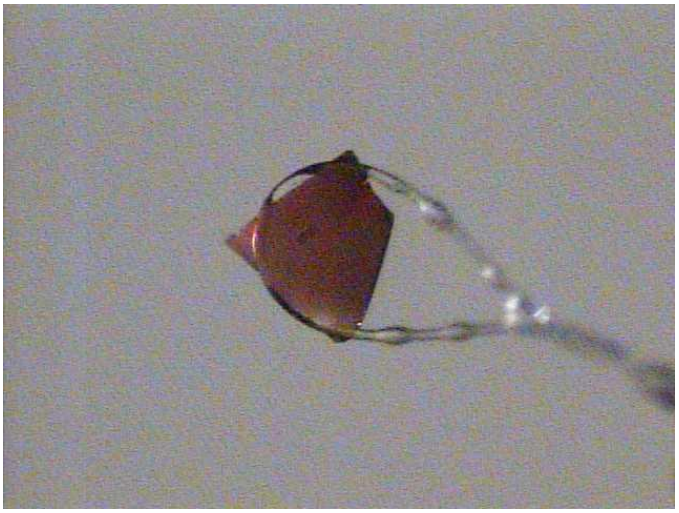

Figure S20. Photograph of single crystal of **5** (size (mm) – 0.1 x 0.1 x 0.08)

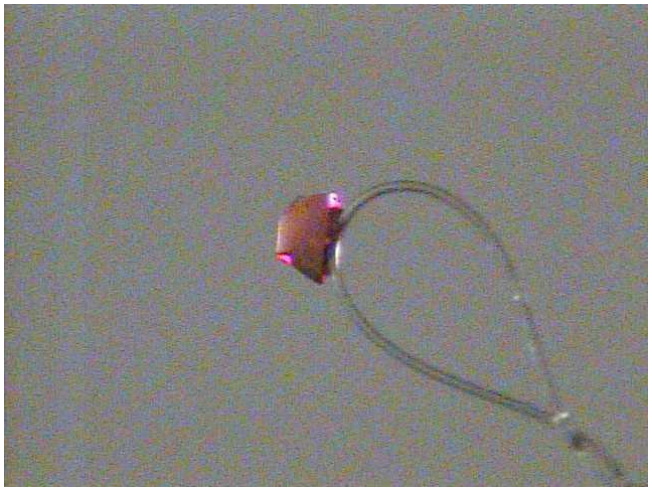

Figure S21. Photograph of single crystal of **6** (size (mm) – 0.05 x 0.32 x 0.36)

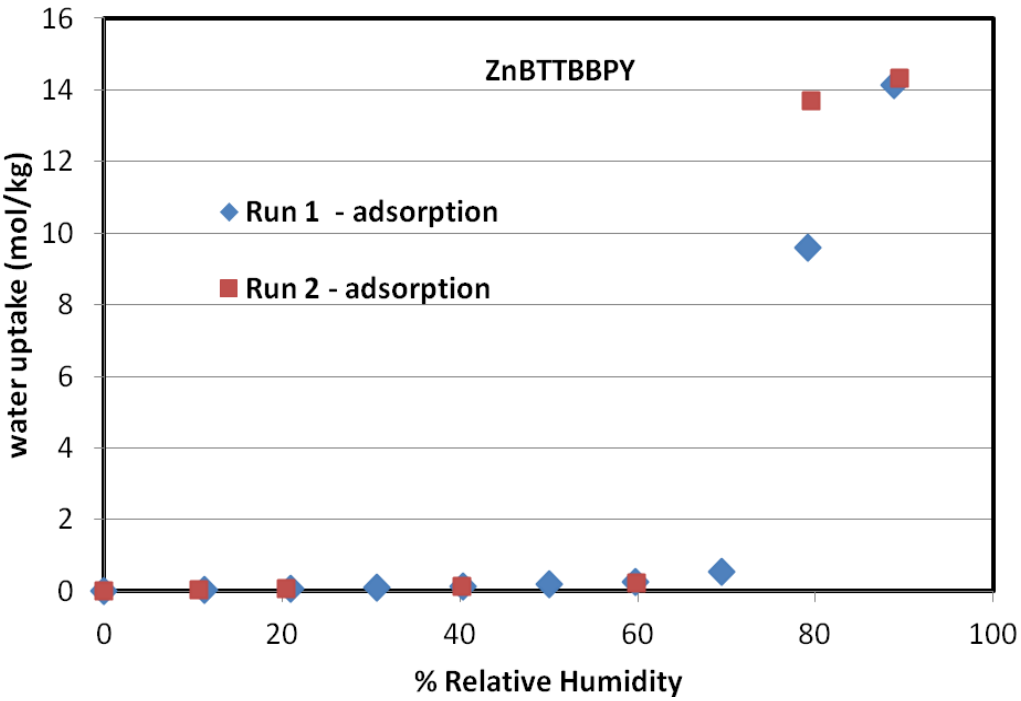

Figure S22. Repeatability of water adsorption isotherms of **4**